IEEE Access
Multidisciplinary | Rapid Review | Open Access Journal

Received 19 June 2022, accepted 2 July 2022, date of publication 6 July 2022, date of current version 13 July 2022.

Digital Object Identifier 10.1109/ACCESS.2022.3188790

RESEARCH ARTICLE

Multiobjective Four-Dimensional Trajectory Synergetic Optimization Based on Congestion Prediction and NSGA3-SA

JINLUN ZHOU, HONGHAI ZHANG, YUFEI WANG, GANG ZHONG, AND HAO LIU
College of Civil Aviation, Nanjing University of Aeronautics and Astronautics, Nanjing 211106, China

Corresponding author: Gang Zhong (anhuizhonggang@126.com)

This work was supported in part by the National Key Research and Development Program of China under Grant 2018YFE0208700, and in part by the National Natural Science Foundation of China under Grant 52002177.

ABSTRACT Synergetic trajectory planning of flights is one of the important goals of trajectory-based operation (TBO), and it is also a method to further improve the utilization of airspace resources with the increasing number of flights in recent years. In order to plan the four-dimensional trajectory (4DT) pre-tactically and comprehensively, match the flight traffic with airspace capacity, reduce congestion, potential conflicts, and fuel consumption thus improving the efficiency of flights, this paper conducts a method for synergetic trajectory planning in the en-route phase from the perspective of airlines. Firstly, the aircraft performance model, aircraft fuel consumption model, and atmospheric model are constructed according to the base of aircraft data (BADA3.11), and an airspace congestion prediction model is constructed based on the historical flow data of airspace. Secondly, a multi-objective synergetic trajectory planning model is established, and a solution method based on the non-dominated sorting genetic algorithm and simulated annealing algorithm (NSGA3-SA) for the problem of synergetic trajectory planning is designed. The simulation shows that the optimization model and the solution algorithm of NSGA3-SA can reduce fuel consumption by about 4.5% compared to the original flight plans and has a good effect on reducing congestion and avoiding conflicts. The running time of the NSGA3-SA can meet the operational requirements of the pre-tactical trajectory planning. The multi-objective optimization model and the solution algorithm proposed in this paper have great value for the research of flight plan optimization.

INDEX TERMS Air traffic management, trajectory-based operation, multi-objective optimization, trajectory planning.

I. INTRODUCTION

Due to the new challenges such as air traffic jams and delays created by the rapid growth of air traffic in recent years, the United States proposed the project Next Generation Transportation System (NextGen) in 2004, and Europe proposed the project Single European Sky ATM Research (SESAR) in 2005. The capacity of information exchange between different aviation departments has improved significantly since then, which also benefits from the improvement of aircraft communication, navigation, surveillance capabilities, and the increasing popularity of trajectory-based operation (TBO).

The associate editor coordinating the review of this manuscript and approving it for publication was Kathiravan Srinivasan.

In 2016, China proposed the plan of Civil Aviation ATM Modernization strategy (CAAMS), which aims to promote the development of the TBO. TBO is not only the direction of civil aviation but also one of the most important goals for the synergetic and refined management of the global air transportation system [1], [2]. Therefore, the synergetic 4-D trajectory planning of aircraft under the TBO environment has become an important research topic in ATM.

According to the different phases of flight procedure performed by the aircraft, the trajectory of the aircraft can be mainly divided into three parts: departure, cruise, and approach. Therefore, the current research on the 4D trajectory optimization of aircraft can be divided into climb trajectory optimization, cruise trajectory optimization, and descent

trajectory optimization according to the differences in the operating stages [3], [4].

The state of aircraft departure is mainly climbing, this phase generally refers to the aircraft starting from the departure end of the runway (DER) to the approved minimum altitude of the air route. The trajectory optimization in the aircraft departure phase usually aims to reduce the consumption of fuel, impact of noise, and control the required time of arrival (RTA) [5]. Wan *et al.* [6] used the new technology of continuous climbing operation (CCO), and the genetic algorithm to optimize the climb path of the aircraft, then carried out an experimental analysis on the parameters of the trajectory optimization model. Prats *et al.* [7] analyzed the influence of noise when the aircraft took off and established a multi-objective trajectory planning model to solve the optimal trajectory. Torres *et al.* [8] adopted a method based on flight procedure design, then combined the performance of different aircraft to design an environmentally friendly departure trajectory with lower emissions and lower noise. Ho-Huu *et al.* [9] adopted a novel climb trajectory optimization method based on the MOEA/D algorithm and also took reducing the influence of take-off noise as the main optimize function to solve the optimal trajectory of climbing, whose conclusion shows that the technology of CCO can reduce the impact of noise significantly.

The cruise phase of an aircraft generally refers to the aircraft starting from the initial cruising waypoint to the initial approach fix (IAF) before the procedure of approach, and the aircraft's state in this phase is mainly level flight. The objectives of trajectory optimization in the cruise phase are usually to reduce the flight distance, balance the airspace capacity, reduce fuel consumption and control the required time of arrival (RTA) of the aircraft [10]–[12]. Seenivasan *et al.* [13] designed a thundercloud circumnavigation method for random weather, which method can realize the rapid trajectory planning of aircraft in the environment of multi-core cumulonimbus and has good real-time performance. Gardi *et al.* [14] combined the task of aircraft trajectory planning with the air traffic management system and proposed a new theory and method of collaborative trajectory planning. Chaimatanan *et al.* [15] combined the network theory with trajectory planning and carried out a model to finish the task of cruise waypoint assignment and design the control time of arrival (CTA) for intercontinental flights. This method has obvious advantages in solving the problem of long-haul flight trajectory planning. Scholars such as Xu and Prats, Tian *et al.*, and Visser [16]–[18] optimized trajectories with the constraints of aircraft performance, and considered both environmental protection and traffic efficiency. Their method of model construction and some conclusions have great significance in the field of trajectory optimization, especially in the cruise phase of aircraft.

The approach phase of the aircraft generally starts from the IAF and ends at the missed approach point (MAPt) or the endpoint of the runway, and the aircraft state in this phase is mainly descending. Trajectory optimization in this phase usually aims to reduce fuel consumption, and noise impact, control the RTA of aircraft and ensure fairness between aircraft [19], [20]. Yang *et al.* [21] considered the airspace structure and the corresponding navigation facilities, then used the NSGA-II algorithm to solve the problem of synergetic flight sequencing and trajectory planning, which obtained good Pareto-optimal front solutions for approach trajectories. Since sustainable transportation is a very important issue for aircraft flight [22], Lim *et al.* [23] takes reducing aircraft fuel consumption as the objective and solves the trajectory of the aircraft in the terminal area, then gives the optimal flight profile for the approaching aircraft theoretically. Sang and John [24] used the new technology of continuous descending operation (CDO) to plan the trajectory of the approaching aircraft, which has positive significance for the promotion of CDO. Cai *et al.* [25] constructed a multi-objective optimization model of approach trajectory, which combined network theory and conflict resolution theory for trajectory planning, and the obtained trajectories have the advantages of no conflict with high efficiency.

Aircraft trajectory prediction is an important basis for aircraft trajectory planning. It cannot only be used for conflict detection between aircraft, but also a key component of flow prediction, and congestion prediction in the airspace. Trajectory prediction methods for civil aviation flights can be classified into three main categories [26]: based on the dynamic model, machine learning model, and flight plan. Deep learning methods have achieved good results in the field of mid-to-long-term prediction trajectory recently, and the dynamic usually has good performance in the short term of trajectory prediction. Ma and Tian [27] proposed a convolution-circular neural network trajectory prediction model which is based on the reconstruction of a convolution neural network and long short-term memory (LSTM). Shi *et al.* [28] proposed a trajectory prediction model based on LSTM that considers the correlation between adjacent trajectory points for long-time trajectory prediction. Wu *et al.* [29] used generative adversarial networks to predict the long-term 4D trajectory of aircraft, which shows the great prospect of deep learning in the field of trajectory prediction. The airspace congestion prediction model in this paper is also based on the framework of deep learning.

The current research on aircraft trajectory planning still has some weaknesses: Firstly, some trajectory optimization models do not consider airspace congestion, which may lead to the implementation of optimized trajectories being affected due to airspace flow restrictions. Secondly, for the multi-objective trajectory optimization problem, the NSGA2 algorithm has the defect of too many kinds of non-dominated optimal solutions when dealing with a problem with more than three objectives. Finally, the ability to search for the optimum solution of the genetic algorithm for decision variables with continuous space is weaker compared to some searching algorithms.

Considering these gaps, this paper constructs a synergetic 4D trajectory optimization model for multi-flights and

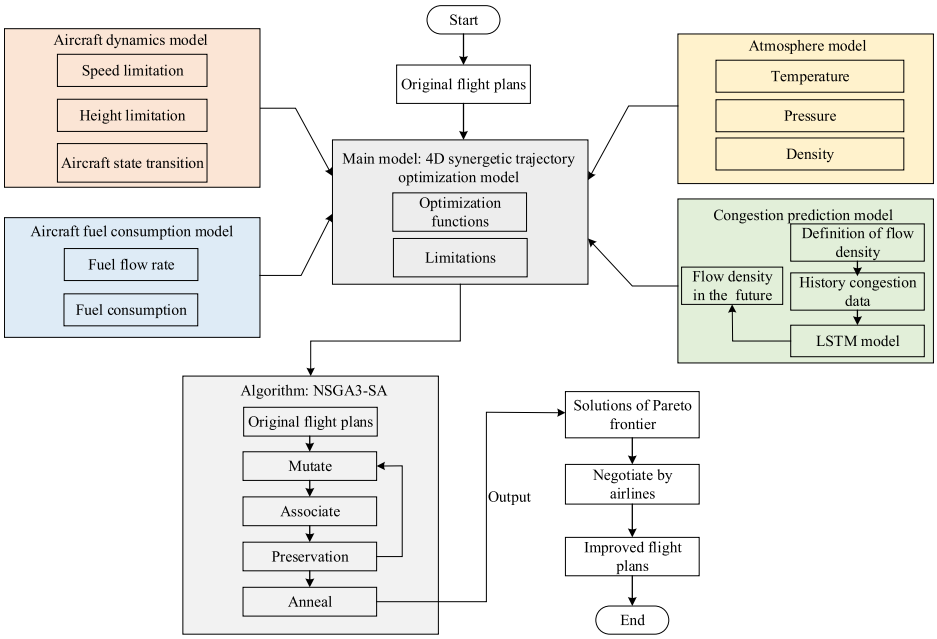

FIGURE 1. The modeling and solution process of this paper.

designs an algorithm of non-dominated sorting based on the reference points and simulated annealing (NSGA3-SA) to solve this model. The main contributions of this research are:

Firstly, a 4D trajectory optimization model is established which comprehensively considers airspace structure, aircraft performance, flight range distance, airspace congestion, fuel consumption, and aircraft conflict. This model and its algorithm can be used to adjust the original flight plan in the pre-tactical stage, reduce the fuel consumption of these flights and improve the operation efficiency while balancing the air traffic flow.

Secondly, the NSGA3-SA algorithm is designed for the multi-objective trajectory optimization model, which has the advantage of solving mixed-integer nonlinear program (MINLP) problems with more than three objective functions (many-objective optimization). At the same time, the simulated annealing algorithm is used for searching for the optimum solutions of continuous variables, which improves the global search ability of this algorithm. In addition, the algorithm maintains a low time complexity and space complexity, which can meet the needs of pre-tactical trajectory planning theoretically.

II. PROBLEM DESCRIPTION AND SYMBOLS

The synergetic 4D trajectory optimization model is based on the TBO environment and aims to optimize the flight plan of multiple flights synergetically. The model and its algorithm are used for selecting the waypoints, determining the required time of arrival, the flight level, and speed for each flight segment of multiple flights. The purpose of synergetic trajectory optimization is to reduce airspace congestion, aircraft fuel consumption, and the possibility of conflict, as well as ensure the punctuality of aircraft.

The input parameters of the 4D trajectory synergetic optimization model in this paper mainly include air traffic flow data, aircraft performance data, meteorological data, and airspace data. Therefore, the model of 4D trajectory synergetic optimization (Section III) requires the atmospheric model in Section III-A, the aircraft dynamics model in Section III-B, the aircraft fuel consumption model in Section III-C, and the congestion prediction model in Section III-D as the support. Then the NSGA3-SA algorithm in Section IV is used to solve the problem of synergetic 4D trajectory optimization. Thus the Pareto frontier solutions are obtained for each airline to negotiate, finally obtaining the optimal 4D trajectory of each flight in Section V. Section VI analyzes the application and performance of the NSGA3-SA algorithm in other typical trajectory planning scenarios The technical route in this paper is shown in Fig. 1:

In this paper, most of the variables that appear in the equations will have their meaning nearby, but some variables that appear multiple times or appear in pseudocode are declared in Table 1. It should be pointed out that all of the subscripts and variables are written in lowercase italics, matrices or vectors are written in uppercase bold italics, sets are written in bold monotype, and functions are written in bold and normal words in this paper.

III. MODELS FOR SYNERGETIC 4D TRAJECTORY PLANNING

A. ATMOSPHERE MODEL

The atmospheric environment model is used to calculate the atmospheric pressure p_{fn}, temperature T_{fn} and atmospheric

TABLE 1. Meaning of the main parameters and symbols.

Symbol	Meaning
t	The subscript of time
n	The subscript of aircraft
i	The subscript of airspace
Lon	Longitude
Lat	Latitude
f_n	The n-th flight
$p_{(lon,lat)}$	The air-way point whose position is (lon,lat)
dep_{fn}	The first air-way point after the departure of f_n
app_{fn}	The last air-way point before the approach of f_n
H_{fn}^{r}	Flight altitude of flight f_n on air-route r
$r_{(p1,p2)}$	The air route between the waypoint p_1 and p_2
fd_i^t	Flow density of the i-th airspace at time t
$\boldsymbol{P}_{fn}$	The air-way point vector selected by the f_n
$\boldsymbol{A}_{fn}$	The vector consists of air-route selected by the f_n
$\boldsymbol{H}_{fn}$	The vector consists of flight altitudes selected by the f_n
$\boldsymbol{V}_{fn}$	The vector consists of speeds selected by the f_n
$\boldsymbol{X}_i$	The i-th feasible solution in the population
$\mathcal{P}_p$	The air-way points adjacent to the air-way point p
$\mathcal{A}$	The set consists of air-routes, $\forall arc_{p(lon,lat),p(lon,lat)} \in \mathcal{A}$
$\mathcal{S}$	The set consists of the airspace boundary, $\forall \boldsymbol{S}_i \in \mathcal{S}$
$\mathcal{F}$	The set consists of flights, $\forall f_n \in \mathcal{F}$
$\mathcal{E}$	The set consists of the Pareto front solution, $\forall \boldsymbol{e}_i \in \mathcal{E}$
$\mathcal{H}$	The set consists of the available flight level, $\forall \boldsymbol{H}_{fn} \in \mathcal{H}$
$\mathcal{G}$	The feasible solution set, $\forall \boldsymbol{X}_i \in \mathcal{G}$
N	Number of flights for synergetic optimization
G	Maximum generation in genetic algorithm
K	Population scale in genetic algorithm
Normalize	The normalize function for optimization objects
Associate	The associate function of the NSGA3
Mutate	The mutate function of the NSGA3
Preservation	The filter function based on the niche count
Anneal	The anneal process of SA

density ρ_{fn} of flight f_n at different positions. These atmospheric parameters are related to aircraft performance and fuel consumption closely. The basic atmosphere parameters are shown in Table 2:

Generally, the atmospheric temperature, pressure, and density can be calculated as (1)(2)(3):

$$T_{fn} = \begin{cases} \mathrm{T}_0 + \beta_{\mathrm{T},<} \cdot h_{fn}, h_{fn} \le \mathrm{h_{trop}} \\ \mathrm{T_{trop}}, h_{fn} > \mathrm{h_{trop}} \end{cases} \tag{1}$$

$$p_{fn} = \begin{cases} p_0 \times \left(\frac{T_{fn} - \Delta T}{\mathrm{T}_0}\right)^{-\frac{\mathrm{g}_0}{\beta_{\mathrm{T},<} \cdot \mathrm{R}}}, h_{fn} \le \mathrm{h_{trop}} \\ p_0 \times \left(\frac{\mathrm{T_{trop}} - \Delta T}{\mathrm{T}_0}\right)^{-\frac{\mathrm{g}_0}{\beta_{\mathrm{T},<} \cdot \mathrm{R}}} \times \mathrm{e}^{-\frac{g_0}{R \cdot \mathrm{T_{trop}}} \times (h_{fn} - \mathrm{h_{trop}})}, \\ h_{fn} > \mathrm{h_{trop}} \end{cases} \tag{2}$$

$$\rho_{fn} = \frac{p_{fn}}{\mathrm{R} \cdot T_{fn}} \tag{3}$$

In Equation (1)(2)(3), T_{fn} is the temperature at the flight f_n' position. h_{fn} is the altitude(m) of the flight f_n. p_{fn} is the air pressure of the flight f_n. ρ_{fn} is the air density at the flight f_n' position. And the parameters such as T_0, p_0, $\beta_{\mathrm{T},<}$, $\mathrm{h_{trop}}$, $\mathrm{T_{trop}}$, g_0, R, Δ T have been illustrated in Table 2.

TABLE 2. Value of atmosphere parameters.

Name	Meaning
κ	Adiabatic index of air, κ = 1.4
R	Real gas constant for air, R = 287.053 ($\mathrm{m^2/K \cdot s^2}$)
g_0	Gravitational acceleration, g_0 = 9.807 ($\mathrm{m/s^2}$)
$\beta_{\mathrm{T},<}$	The altitude temperature gradient, $\beta_{\mathrm{T},<}$ = -0.065 (K/m)
T_0	ISA atmospheric temperature at MSE, T_0 = 288.15 (K)
$\mathrm{T_{trop}}$	The temperature of tropopause, $\mathrm{T_{trop}}$ = 1216.65 (K)
ΔT	The temperature difference between the International Standard Atmosphere (ISA) and the true atmosphere
p_0	ISA atmospheric pressure at MSL, p_0 = 101325 (pa)
ρ_0	ISA atmospheric density at MSL, ρ_0 = 1.225 ($\mathrm{kg/m^3}$)
a_0	ISA speed of sound, a_0 = 340.29 (m/s)
$\mathrm{h_{trop}}$	The altitude of the tropopause, $\mathrm{h_{trop}}$ = 11000 (m)

The speed of the wind and the temperature of different positions is read from the European Centre for Medium-range Weather Forecasts (ECMWF), as (4):

$$V_{\mathrm{w},(lon,lat)}, \Delta T_{(lon,lat)} = \mathrm{dataframe}(lon, lat) \tag{4}$$

In Equation (4), $V_{\mathrm{w},(\mathrm{lon,lat})}$ is the speed of the wind at the position whose longitude is lon and latitude is lat. $\Delta \mathrm{T}_{(lon,lat)}$ is the temperature difference between the international standard atmosphere (ISA) and the true atmosphere.

B. AIRCRAFT DYNAMICS MODEL

The aircraft aerodynamic model is constructed based on the base of aircraft data 3.11 (BADA 3.11), and the relevant performance parameters of B747-400 (as shown in Table 3) are used as an example to illustrate the aircraft dynamics model [30], [31].

TABLE 3. Fuel parameters and values of B747-400.

Symbol	Value (unit)
$\mathrm{M_{ref}}$	366.33 (t)
$\mathrm{S_{wing}}$	510.97 ($\mathrm{m^2}$)
g_0	9.807 ($\mathrm{m/s^2}$)
$\mathrm{cd_{0cr}}$	0.025669
$\mathrm{cd_{2cr}}$	0.039082
$\mathrm{C_{TC,1}}$	759790
$\mathrm{C_{TC,2}}$	52423
$\mathrm{C_{TC,3}}$	$0.40968 * 10^{-10}$

The drag of the aircraft can be calculated by (5).

$$Drag = \frac{1}{2}\rho_{fn} \cdot V_{fn}^2 \cdot \mathrm{S_{wing}} \times \left(\mathrm{cd_{0cr}} + \mathrm{cd_{2cr}}\left(\frac{2M_{fn} \cdot \mathrm{g}_0}{\rho_{fn} \cdot \mathrm{S_{wing}} \cdot V_{fn}^2}\right)^2\right) \tag{5}$$

In Equation (5), $Drag$ represents the drag of the aircraft, $\mathrm{S_{wing}}$ is the wing area of the aircraft, $\mathrm{M_{ref}}$ is the reference mass of the aircraft, $\mathrm{cd_{0cr}}$, $\mathrm{cd_{2cr}}$ is the performance parameters in BADA 3.11, V_{fn} is the true airspeed (TAS) of the aircraft. And the meaning of some parameters such as ρ_{fn}, g_0 has been explained in Table 2.

The thrust of the aircraft has the constraint of (6).

$$Thr \leq C_{\mathrm{Tc},1} \times \left(1 - \frac{h_{fn}}{C_{\mathrm{Tc},2}} + C_{\mathrm{Tc},3} \cdot h_{fn}^2\right) \tag{6}$$

In Equation (6), Thr represents the thrust of the aircraft, $C_{TC,1}$, $C_{TC,2}$, $C_{TC,3}$ are both the thrust parameters given by the BADA3.11, which are used to determine the maximum thrust of the aircraft in different altitudes. h_{fn} is the altitude (km) of the flight f_n.

The rate of climb or descent (ROCD) can be calculated by (7).

$$ROCD = \frac{\mathrm{d}h}{\mathrm{d}t} = \frac{T_{fn} - \Delta T}{T_{fn}} \times \left[\frac{(Thr - Drag) \cdot V_{fn}}{M_{fn} g_0}\right] \times \left[1 + \left(\frac{V_{fn}}{g_0}\right) \cdot \frac{\mathrm{d}V_{fn}}{\mathrm{d}h_{fn}}\right]^{-1} \tag{7}$$

In Equation (7), ROCD represents the rate of climb or descent. And the pitch angle of the aircraft θ can be calculated by (8).

$$\theta = \arcsin\left(\frac{ROCD}{V_{fn}}\right) \tag{8}$$

According to the force analysis of the aircraft in the direction perpendicular to the roll axis and parallel to the roll axis, the gravity and lift of the aircraft perpendicular to the roll axis are balanced, and the thrust, drag, and gravity parallel to the roll axis produce the acceleration of the aircraft, as (9).

$$\begin{cases} Thr + Drag + M_{fn} \cdot g_0 \cdot \sin\theta = M_{fn} \cdot a_{fn} \\ m \cdot g_0 \cdot \cos\theta = \frac{1}{2}\rho_{fn} \cdot V_{fn}^2 \cdot \mathrm{S_{wing}} \cdot \frac{2M_{fn} \cdot g_0}{\rho_{fn} \cdot \mathrm{S_{wing}} \cdot V_{fn}^2} \end{cases} \tag{9}$$

Therefore, the displacement of the aircraft can be calculated by the aircraft speed V_{fn}, acceleration a_{fn}, and $ROCD$, as (10)(11).

$$x_{t_2} = x_{t_1} + \int_{t_1}^{t_2} \left(V_{fn,t_1} - V_{\mathrm{w},(lon,lat)} \cdot \cos\alpha + \int_{t_1}^{t_2} a_{fn,t_1} \cdot \cos\theta \mathrm{d}t\right) \mathrm{d}t \tag{10}$$

$$h_{t_2} = h_{t_1} + \int_{t_1}^{t_2} ROCD \mathrm{d}t \tag{11}$$

In Equation (10)(11), $\boldsymbol{x}_{t2}$ represents the new position (longitude, latitude) of the aircraft at time t_2, h_{t2} means the new position (altitude) of the aircraft at t_2, $\boldsymbol{x}_{t1}$ represents the original position (longitude, latitude) of the aircraft at t_1, h_{t1} means the original position (altitude) of the aircraft at t_1, α is the component of wind speed parallel to the airway, and $V_{\mathrm{w},(lon,lat)}$ is the speed of the wind at the position whose longitude is lon and latitude is lat.

Finally, the aircraft speed in the cruise phase is mainly represented by the Mach number. The conversion between Mach number and V_{fn} is as follows:

$$V_{fn} = Mach_{fn} \cdot \sqrt{\kappa \cdot \mathrm{R} \cdot T_{fn}} \tag{12}$$

In Equation (12), $Mach_{fn}$ is the Mach number of flight f_n, T_{fn} is the Temperature of flight fn. The parameters such as κ and R have been explained in Table 2.

C. AIRCRAFT FUEL CONSUMPTION MODEL

The aircraft fuel consumption model is constructed based on BADA 3.11 too, and the relevant performance parameters of B747-400 (as shown in Table 4) are used as an example to illustrate the model.

TABLE 4. Value of fuel parameters of B747-400.

Symbol	Value (unit)
$\mathrm{M_{ref}}$	366.33 (t)
$\mathrm{S_{wing}}$	510.97 ($\mathrm{m^2}$)
$\mathrm{g_0}$	9.807 ($\mathrm{m/s^2}$)
$\mathrm{cf_1}$	0.58259
$\mathrm{cf_2}$	1283.9
$\mathrm{cf_3}$	45.38
$\mathrm{cf_4}$	72929
$\mathrm{cd_{0cr}}$	0.025669
$\mathrm{cd_{2cr}}$	0.039082
$\mathrm{cf_{cr}}$	0.89625

Firstly, the drag and the thrust of the aircraft can be calculated by (13). Thus the fuel flow rate (kg/min) of the aircraft can be calculated by (14) and the fuel consumption of the aircraft can be calculated by (15).

$$Thr = \begin{cases} Drag, \text{Cruise } (\theta = 0) \\ Drag + \mathrm{M}_{fn} \cdot g_0 \cdot \sin\theta, \text{Climb } (\theta > 0) \\ Drag + \mathrm{M}_{fn} \cdot g_0 \cdot \sin\theta, \text{Descend } (\theta < 0) \end{cases} \tag{13}$$

$$ff\,(\mathrm{kg/min}) = \begin{cases} \mathrm{cf_1} \cdot \mathrm{cf_{cr}} \times \left(1 + \frac{V_{fn}}{\mathrm{cf_2}}\right) \times Thr, \text{Cruise} \\ \mathrm{cf_1} \times \left(1 + \frac{V_{fn}}{\mathrm{cf_2}}\right) \cdot Thr, \text{Climb} \\ \max\left(\mathrm{cf_1} \cdot \left(1 + \frac{V_{fn}}{\mathrm{cf_2}}\right) \cdot Thr, \mathrm{cf_3} \cdot \left(1 - \frac{H_{fn}}{\mathrm{cf_4}}\right)\right), \\ \text{Descend} \end{cases} \tag{14}$$

$$fc = \int ff \mathrm{d}t \tag{15}$$

In Equations (13)(14)(15), some parameters such as $Drag$, Thr, V_{fn}, H_{fn} have been explained before. Parameters such as $\mathrm{cf_1}$, $\mathrm{cf_{cr}}$, $\mathrm{cf_2}$ and $\mathrm{cf_4}$ are hyper-parameters given by the BADA3.11. And ff is the fuel flow rate (kg/min) of the aircraft and fc is the fuel consumption of the aircraft.

Finally, the mass of the aircraft will change with the fuel consumption, which is:

$$M_{fn} = M_{fn} - \delta \cdot \int ff dt \tag{16}$$

In Equation (16), M_{fn} is the mass of flight f_n, and δ is the density of the aviation fuel, we take $\delta = 780$ ($\mathrm{kg/m^3}$).

D. CONGESTION PREDICTION MODEL

1) FLOW DENSITY

Flow density is a concept proposed in this paper to evaluate the congestion of the airspace. The traditional method to evaluate the congestion of airspace quantitively requires a critical value of the airspace capacity. But the calculation of airspace capacity requires other information such as air-route structure, number of controllers, and navigation facilities.

Those data are hard to collect and the process of evaluating the capacity is different between different control zones. This paper proposes the concept of flow density to evaluate airspace congestion, calculated by (17):

$$fd_i^t = \frac{flow_i^t}{S_i} \tag{17}$$

In Equation (17), fd_i^t is the flow density of the i-th airspace in time t (hour). $flow_i^t$ is the total running time (s) of aircraft in the i-th airspace in time t (hour). S_i is the area (km^2) of the i-th airspace. From the definition of the flow density, it can be found that this indicator not only considers the flight time in the airspace (time, hour) but also considers the capacity of the airspace (area, km^2). The concept of flow density is used as an indicator for measuring the degree of airspace congestion in this paper.

Although the calculation of the flow density index is succinct and can reflect the airspace congestion intuitively. However, there are some problems when measuring airspace congestion with flow density:

First of all, the flight time of a flight is related to the length of the airway in the airspace directly, rather than the area of airspace. The larger the airspace area, the longer the route in the airspace and the total flight time, but it can be found that the increase of the area has a quadratic relationship to distance and flight time. Therefore, the value of flow density will be smaller than its actual degree of congestion when the airspace is too large as shown in Fig. 2.

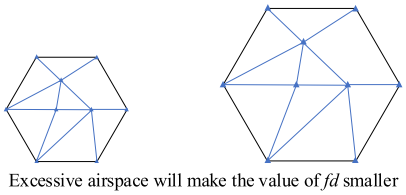

FIGURE 2. Excessive airspace generates an error in flow density.

Secondly, when the distribution of routes in the airspace is uneven, the value of flow density will be smaller than the actual airspace congestion, as shown in Fig. 3:

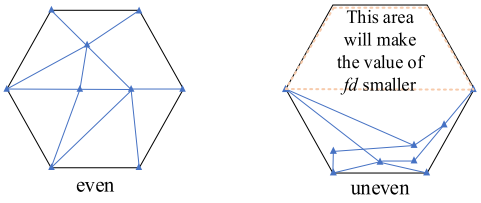

FIGURE 3. Uneven routes in airspace generate an error in flow density.

When the routes in the airspace are concentrated in a certain part of the airspace, there will be an error in the flow density. However, due to the environmental needs of the control work and the limitation of the workload of controllers, the situation shown in Fig. 2 and 3 does not comply with the airspace delineation regulations. Here are three airspace delineation rules used in China that are used to illustrate the unreasonableness of these airspaces [32]:

1. "The setting of the control sector should help the controller to control all flight activities in a specific area so that the controller will not be disturbed too much."

2. "The designation of radar control sectors should help the controller to focus on the radar screen, reduce the interference of the video images on the radar screen to the controller, and reduce the workload by coordination."

3. "Select some busy routes according to the distribution of conflict points then allocate to the corresponding control sectors reasonably, which enables the controller to focus on these main routes and to achieve an even workload."

Due to the general rules and regulations followed by airspace designation, the intersection points are generally near the center of the airspace. There are usually no such situations of large airspace containing a large number of air routes or airspace with a very uneven distribution of air routes. So it can be considered that when the airspace size is appropriate and the routes are evenly distributed in the airspace, flow density is a good indicator to reflect the degree of airspace congestion.

2) STRUCTURE OF THE LSTM PREDICTION MODEL

LSTM is a type of recurrent neural network (RNN) composed of LSTM memory units. Due to the structure of the LSTM unit, the LSTM has the advantage to extract the feature of time series data.

The model of LSTM is used to predict the flow density of different airspace at different times. The objective of the model is minimum the mean absolute error (MAE), and the loss function is (18):

$$\min MAE = \sum_{i=1}^{N}\sum_{t=0}^{23}\left|fd_i^t - fd_i^{'t}\right|, fd_i^t = \Phi_i(t; W) \tag{18}$$

In Equation (18), fd_i^t is the flow density of the i-th airspace at time t, which is predicted by the LSTM model Φ with the weight matrix $\boldsymbol{W}$. fd'^t_i is the actual historical value of the flow density of the i-th airspace at time t. The structure of the LSTM model can be described by (19a-19f).

$$i_t = \text{sigmoid}\left(W_{xi}^{\mathrm{T}} \otimes x_t + W_{hi}^{\mathrm{T}} \otimes h_{t-1} + b_i\right) \tag{19a}$$

$$f_t = \text{sigmoid}\left(W_{xf}^{\mathrm{T}} \otimes x_t + W_{hf}^{\mathrm{T}} \otimes h_{t-1} + b_f\right) \tag{19b}$$

$$o_t = \text{sigmoid}\left(W_{xo}^{\mathrm{T}} \otimes x_t + W_{ho}^{\mathrm{T}} \otimes h_{t-1} + b_o\right) \tag{19c}$$

$$c'_t = \tanh\left(W_{xc}^{\mathrm{T}} \otimes x_t + W_{hc}^{\mathrm{T}} \otimes h_{t-1} + b_c\right) \tag{19d}$$

$$c_t = f_t \otimes c_{t-1} + i_t \otimes c'_t \tag{19e}$$

$$Y_t = h_t = o_t \otimes \tanh(c_t) \tag{19f}$$

In Equations (19a-19f), $\boldsymbol{W}_{xi}$, $\boldsymbol{W}_{xf}$, $\boldsymbol{W}_{xo}$, $\boldsymbol{W}_{xc}$ are weight matrices of the corresponding gate which connected to the input matrix $\boldsymbol{x}_t$. $\boldsymbol{W}_{hi}$, $\boldsymbol{W}_{hf}$, $\boldsymbol{W}_{ho}$, $\boldsymbol{W}_{hc}$ are weight matrices that are connected to the short-term state $\boldsymbol{h}_{t-1}$, b_i, b_f, b_o, b_c are

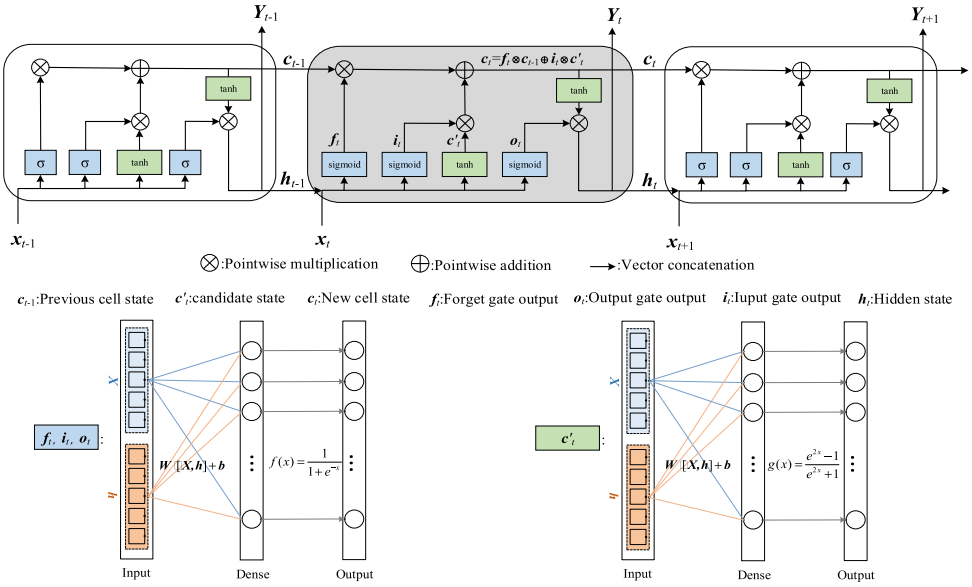

FIGURE 4. The structure of the LSTM model.

bias corresponds to each gate.σ is the activation function of Sigmoid (which is $f(x) = (1+e^{-x})-1$), tanh is the activation function of tanh (which is $g(x) = (e^{2x}\text{-}1) / (e^{2x}+1)$). $\boldsymbol{f}_t$ is the forget gate of the LSTM model, $\boldsymbol{i}_t$ and $\boldsymbol{o}_t$ are the input gate and output gate of the LSTM model, $\boldsymbol{c}_t$ and $\boldsymbol{c}'_t$ are the gates used to memorize the characteristics of the input samples. $\otimes$ represents the dot product between two matrices, and T represents the transpose operation of a matrix. The structure of the LSTM prediction model is shown in Fig. 4 [33], [34]:

E. FOUR-DIMENSIONAL TRAJECTORY SYNERGETIC OPTIMIZATION MODEL

1) DECISION VARIABLES

For every flight in this 4-D trajectory optimization problem, three main variables need to be determined by the model and its algorithm. The vector $\boldsymbol{P}_{fn}$ consists of air-way points selected by the n-th flight, the vector $\boldsymbol{H}_{fn}$ consists of flight altitudes selected by the n-th flight, and the vector $\boldsymbol{V}_{fn}$ consists of speeds selected by the n-th flight. For every flight, the length of its solution vector has the equation that $||\boldsymbol{P}_{fn}||_0 = ||\boldsymbol{H}_{fn}||_0+1 = ||\boldsymbol{V}_{fn}||_0+1$. The solution vector $\boldsymbol{x}_{fn}$ of flight f_n is:

$$x_{fn} = \left[P_{fn}, H_{fn}, V_{fn}\right]^{\mathrm{T}} \tag{20a}$$

$$J = \left\|H_{fn}\right\|_0 = \left\|V_{fn}\right\|_0 \tag{20b}$$

$$P_{fn} = [p_1, p_2, \ldots p_{J+1}], H_{fn} = [h_1, h_2, \ldots, h_J],$$

$$V_{fn} = [v_1, v_2, \ldots v_J] \tag{20c}$$

So the solution matrix composed of all of the flights is $\boldsymbol{X}$, as (21):

$$X = \left[x_{f1}, x_{f2}, \ldots, x_{fn}\right]^{\mathrm{T}} \tag{21}$$

It should be pointed out that the optimized flight plan is only for the cruising phase of the aircraft, which excludes the phase of departure and the approach.

2) OBJECTIVE FUNCTIONS

a: MINIMUM TOTAL FLIGHT RANGE

The flight range is closely related to fuel consumption and flight time. Therefore, a smaller flight range of the aircraft is pursued to obtain more benefits in general flight planning. This objective can be calculated as (22):

$$\min Z_1 = \sum_{n=1}^{\mathrm{N}} \sum_{j=0}^{J} \left\|p_j, p_{j+1}\right\|_2, p_j \in P_{fn} \tag{22}$$

b: MINIMUM TOTAL FUEL CONSUMPTION

Aircraft fuel consumption directly affects airline efficiency and environmental protection-related issues. Generally, fuel consumption is closely related to aircraft altitude selection and cruising speed. This objective can be calculated as (23):

$$\min Z_2 = \sum_{n=1}^{\mathrm{N}} \sum_{j=0}^{J} \mathrm{fc}(\left\|p_j, p_{j+1}\right\|), p_j \in P_{fn} \tag{23}$$

In Equation (23), fc represents the fuel consumption function from waypoint p_j to p_{j+1}, and the process of calculating the fuel consumption has been described in Section III-C.

c: MINIMUM POTENTIAL CONFLICTS

Conflicts can be avoided by adjusting the vertical separation between aircraft usually. However, if conflicts can be avoided by ensuring the horizontal and lateral separation between aircraft in the pre-tactical trajectory planning stage, it is very beneficial to reduce the control workload and airspace

congestion [3]. This objective can be calculated as (24) and (25):

$$\min Z_3 = \sum_{n_1=1}^{N} \sum_{n_2=n_1+1}^{N} \sum_{t=0}^{23} \sum_{p_{(lon,lat)} \in P_{fn1} \cup P_{fn2}} \times \text{conflict}\left(p_{(lon,lat)}, p_{fn_1,t}, p_{fn_2,t}\right) \tag{24}$$

$$\text{conflict}(p_{(lon,lat)}, p_{fn_1,t}, p_{fn_2,t}) = \begin{cases} 1, \text{if } \left| \left\| p_{(lon,lat)} - p_{fn1,t} \right\|_2 - \left\| p_{(lon,lat)} - p_{fn2,t} \right\|_2 \right| \\ \leq 10\text{km} \\ 0, \text{Else} \end{cases} \tag{25}$$

d: MINIMUM THE CONGESTION

This objective function aims to balance the airspace flow by making the aircraft avoid the most congested airspace moments as much as possible. This objective can be calculated as:

$$\min Z_4 = \sum_{n=1}^{N} \sum_{i=1}^{I} fd_i^t \tag{26}$$

In Equation (26), fd_i^t is the flow density of the i-th airspace in time t (hour), N is the number of the flight, and I is the number of airspaces crossed by flights.

e: MINIMUM THE DIFFERENCE BETWEEN THE REQUIRED TIME OF ARRIVAL (RTA) AND CONTROLLED TIME OF ARRIVAL (ATA)

In this paper, the *RTA* represents the time schedule of the flight in the original flight plan, and the *CTA* is the time schedule of the flight in the flight after optimization. This objective function is designed to ensure the punctuality of the aircraft [36]. This objective can be calculated as:

$$\min Z_5 = \sum_{p \in arr \cup dep} \sum_{n=1}^{N} \left| RTA_{fn}^p - CTA_{fn}^p \right| \tag{27}$$

In Equation (27), RTA_{fn}^p is the required time of arrival for the waypoint p in the original flight plan of f_n. CTA_{fn}^p is the controlled time of arrival for the waypoint p in the optimized flight plan of f_n. The waypoints p belong to the set of app and dep, which is composed of the last waypoints before the approach and the first waypoints after the departure of the flights in set $\boldsymbol{\mathcal{F}}$.

3) CONSTRAINTS

a: CONSTRAINTS OF WAYPOINT SELECTION

Firstly, all flights start from their first waypoint after departure and end at their last waypoint before approach, thus the first element of the list $\boldsymbol{P}_{fn}$ should be the first cruise waypoint of the flight, and the last element of the list $\boldsymbol{P}_{fn}$ should be the approach waypoint of the flight, as (28):

$$P_{fn}[0] = dep_{fn}; P_{fn}[-1] = app_{fn} \tag{28}$$

Secondly, the next waypoint selected by the flight should be adjacent to the current waypoint, as (29)(30):

$$A(j,k) = \begin{cases} 1, \exists r_{p_j,p_k} \leq \infty \\ 0, \forall r_{p_j,p_k} = \infty \end{cases} \tag{29}$$

$$p_{k=j+1} \in \boldsymbol{\mathcal{P}}, \forall A(j,k) = 1 \tag{30}$$

b: CONSTRAINTS OF FLIGHT LEVEL SELECTION

Firstly, the flight level should be higher than the minimum safe altitude of the airspace (MSA), and lower than the maximum altitude allowed by the airspace h_{c_max} and ceiling of the certain aircraft h_{MO}, as (31):

$$MSA_i \leq H_{fn}^r \leq \min\left\{h_{MO}, h_{c\_max}\right\} \tag{31}$$

Secondly, the flight level selected by the aircraft should be compliant with the principle of airspace management. This paper chooses levels of odd-numbered for eastbound flights and even-numbered for westbound, as (32)(33).

$$H_{fn} \subseteq \boldsymbol{\mathcal{H}}_{2k+1}, \text{if} V_{fn} \geq 0, k \in N^+ \tag{32}$$

$$H_{fn} \subseteq \boldsymbol{\mathcal{H}}_{2k}, \text{if} V_{fn} < 0, k \in N^+$$

$$\forall H_{fn}^r \in H_{fn} \tag{33}$$

c: CONSTRAINTS OF SPEED ADJUSTMENT

The speed of the aircraft should be less than the max operation Mach number M_{MO} of certain aircraft and more than the parameter calculated by $C_{Vmin} \cdot V_{stall}$ (C_{Vmin} and V_{stall} of each aircraft are announced in BADA), as (34):

$$C_{Vmin} \cdot V_{stall} \leq V_{fn} \leq \sqrt{\kappa \cdot R \cdot T_{fn}} \cdot M_{MO} \tag{34}$$

d: CONSTRAINT OF THE CLIMB OR DESCEND RATE

The absolute value of climb or descend distances in a certain time t should be less than the maximum rate of climb or descend ($ROCD_{max}$) for a certain aircraft, as (35):

$$\left| \Delta h_{fn,t} \right| \leq ROCD_{max} \cdot V_{fn} \cdot t \tag{35}$$

e: CONSTRAINTS OF AIRCRAFT PUNCTUALITY

The difference between the controlled time of arrival and the required time of arrival should be in the range of the maximum acceptable advance (MAA) and the maximum acceptable delay (MAD), as (36):

$$MAA \leq ATA_{fn}^p - CTA_{fn}^p \leq MAD, f_n \in \boldsymbol{\mathcal{F}}, p \in \{arr, dep\} \tag{36}$$

Finally, some parameters used in the constraints of the model are displayed in Table 5:

4) ANALYSIS OF THE MODEL

In summary, the multi-objective 4D trajectory synergetic optimization model can be described as follows:

$$\min Z_1 = \sum_{n=1}^{N} \sum_{j=0}^{J} \left\| p_j, p_{j+1} \right\|, p_j \in P_{fn}$$

TABLE 5. Some parameters used for the constraints.

Symbol	Value (unit)
C_{Vmin} (B747-400)	1.3
V_{stall} (B747-400)	165 (kt)
M_{MO} (B747-400)	0.92
h_{MO} (B747-400)	45000 (ft)
$h_{c\ max}$	34998 (ft)
MAA	300 (s)
MAD	300 (s)

$$\min Z_2 = \sum_{n=1}^{N}\sum_{j=0}^{J} fc(\|p_j, p_{j+1}\|), p_j \in P_{fn}$$

$$\min Z_3 = \sum_{n_1=1}^{N}\sum_{n_2=n_1+1}^{N}\sum_{t=0}^{23}\sum_{p_{(lon,lat)}\in P_{fn1}\cup P_{fn2}} \times \text{conflict}\left(p_{(lon,lat)}, p_{fn_1,t}, p_{fn_2,t}\right)$$

$$\min Z_4 = \sum_{n=1}^{N}\sum_{i=1}^{I} fd_i^t$$

$$\min Z_5 = \sum_{p\in arr\cup dep}\sum_{n=1}^{N}\left|RTA_{fn}^p - ATA_{fn}^p\right|$$

$$\text{s.t.}\begin{cases} P_{fn}[0] = dep_{fn}; P_{fn}[-1] = app_{fn} \\ A(j,k) = \begin{cases} 1, \exists r_{p_j,p_k} \le \infty \\ 0, \quad \forall r_{p_j,p_k} = \infty \end{cases} \\ p_{k=j+1} \in \boldsymbol{\mathcal{P}}, \quad \forall A(j,k) = 1 \\ MSA_i \le H_{fn} \le \min\left\{h_{MO}, h_{c\_max}\right\} \\ H_{fn} \subseteq \boldsymbol{\mathcal{H}}_{2k+1}, \text{ if } V_{fn} \ge 0, k \in N^+ \\ H_{fn} \subseteq \boldsymbol{\mathcal{H}}_{2k}, \text{ if } V_{fn} < 0, k \in N^+ \\ C_{Vmin}\cdot V_{stall} \le V_{fn} \le V_{MO} \\ \quad \forall H_{(p_1,p_2)} \in H_{fn}, \quad \forall r_{(p_1,p_2)} \in \boldsymbol{\mathcal{A}} \\ \left|\Delta h_{fn,t}\right| \le ROCD_{max}\cdot V_{fn}\cdot t \\ MAA \le ATA_{fn}^p - RTA_{fn}^p \le MAD, f_n \in \boldsymbol{\mathcal{F}}, \\ p \in \{arr, dep\} \end{cases}$$

The algorithmic complexity of the aircraft trajectory optimization problem increases exponentially with the increase of decision variables. Therefore, it is very important to design a suitable heuristic algorithm to solve this mixed-integer nonlinear problem (MINLP). NSGA2 can solve this kind of model quite well, but it also has some shortcomings: for multi-objective optimization, the number of non-dominated solutions increases exponentially with the increase of the objective function, resulting in the poor diversity of the final results obtained by this algorithm. In addition, the search performance based on the genetic algorithm or its improved methods for continuous variables, such as the search for the optimal speed of aircraft (continuous variables) is usually not accurate and not good enough. Considering these problems, this paper designs an algorithm of NSGA3-SA to solve this mixed-integer nonlinear optimization problem better.

IV. ALGORITHMS

A. ADAM WEIGHT UPDATE ALGORITHM FOR LSTM OF THE CONGESTION PREDICTION MODEL

The optimizer for the training of the LSTM prediction model is Adam, which is an adaptive weight update method used widely [37], [38] in the field of deep learning. The pseudocode of Adam is shown in Table 6:

TABLE 6. Adam weight update algorithm of LSTM.

Algorithm1: Adam weight update algorithm of LSTM.
Input: historical time series data of flow density $\boldsymbol{H}_t$.
Output: trained flow density prediction model $\Phi(\cdot;\boldsymbol{W})$.
Hyper-parameters: training epochs K, β_1=0.9, β_2=0.999, η=0.001.
Initialize: Initialize weights $\boldsymbol{W}$ as random numbers; Initialize intermediate variables v_k, m_k, v'_k, m'_k as random numbers; k=0.
While k < K:
$\boldsymbol{L} = \boldsymbol{H}_t - \Phi(\boldsymbol{t}_p;\boldsymbol{W})$
$m_k = \beta_1\cdot m_{k-1} + (1-\beta_1)\cdot\Delta\boldsymbol{L}/\Delta\boldsymbol{W}$
$v_k = \beta_2\cdot v_{k-1} + (1-\beta_2)\cdot(\Delta\boldsymbol{L}/\Delta\boldsymbol{W})\otimes(\Delta\boldsymbol{L}/\Delta\boldsymbol{W})$
$m'_k = m_k/(1-\beta_1)$
$v'_k = v_k/(1-\beta_2)$
$\boldsymbol{W} = \boldsymbol{W} - \eta\cdot m'_k/(v'_k)^{1/2}$
$k = k+1$

In Table 6, β_1, β_2 are hyperparameters setting for the weight update iteration, $\boldsymbol{L}$ is the loss function, η is the step size, $\boldsymbol{W}$ is the weight matrix of the hidden layers for deep learning, k is the number of iterations, m_k, v_k, m'_k, v'_k are intermediate variables that play the role of passing parameters, $\Delta L/\Delta\boldsymbol{W}$ is the partial derivative of the loss function $\boldsymbol{L}$ to the weight matrix $\boldsymbol{W}$. $\bigotimes$ represents the dot product between two matrices. The output of this algorithm is the prediction model $\Phi(\cdot;\boldsymbol{W})$, whose input data is a set of time-series data $\boldsymbol{t}$. The time-series data $\boldsymbol{t}$ is composed of the timestamps t and the congestion data fd, whose configure is $[(t_1, t_2,\ldots,t_p), (fd_1, fd_2,\ldots fd_p)]$. Finally, the output of the prediction model is the congestion data, which can be calculated by $fd_{p+1} = \Phi(\boldsymbol{t}_p;\boldsymbol{W})$.

B. NSGA3-SA FOR FOUR-DIMENSIONAL TRAJECTORY SYNERGETIC OPTIMIZATION MODEL

The NSGA3-SA algorithm consists of two main parts: for the discrete variables $\boldsymbol{P}_{fn}$ of the waypoints selection and discrete variables $\boldsymbol{H}_{fn}$ of the flight levels selection, the NSGA3 algorithm is used to search for the optimal solution by sorting based on reference points. For the continuous variables $\boldsymbol{V}_{fn}$ of flight speed selection, the SA algorithm is used to search for the optimal cruise speed of the aircraft based on the Metropolis principle [39]. From the perspective of an algorithm, this algorithm is suitable for multi-flight synergetic trajectory planning which has both discrete and continuous decision variables while it is a many-objective optimization problem. In other words, the algorithm designed for this problem can be seen as a combination of two different algorithms of NSGA3 and SA, because each algorithm has its advantage in searching for different scenarios. The general steps of NSGA3-SA are shown in Fig. 5:

The pseudocode of NSGA3-SA is shown in Table 7:

There are some functions described in Table7 such as **Cross and mutate**, **Normalize**, **Associate**, etc. These functions will be described in detail in the following tables of this paper. All of the pseudocode is written in Python's

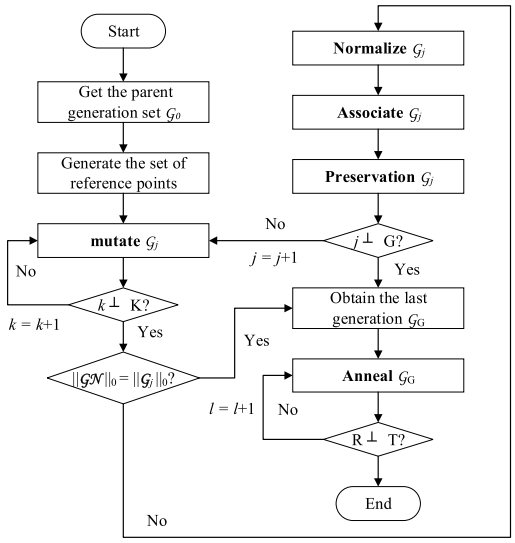

FIGURE 5. The steps of the NSGA3-SA algorithm.

TABLE 7. The algorithm pseudocode of NSGA3-SA.

Algorithm2: **NSGA3-SA**
Input: reference points set $\mathcal{Z}$, parent generation set $\mathcal{G}_0$
Output: the last generation $\mathcal{G}_G$ of solutions (Pareto front solutions)
Hyper-parameters: G, K, L
Initialize: $j = 0$, $k = 0$, $l = 0$, G = 200, $K = 20$, $L = 200$
$\mathcal{Z}$ = reference points set generated by Algorithm3
While $j \le$ G:# the algorithm of NSGA3
  $\mathcal{GN} = \mathcal{G}_j$
  While $k \le K$:
    $g = \mathcal{GN}$
    q = **Cross and mutate**(g) #the recombination and mutation operation for g
    $\mathcal{GN} \cup q$
    $k = k+1$
  If $||\mathcal{GN}||_0 = ||\mathcal{G}_j||_0$:
    $\mathcal{G}_j = \mathcal{G}_j$, **Break to** the algorithm of SA
  Else:
    $\mathcal{G}_j = \mathcal{GN}$
    $\mathcal{G}_j$ = **Normalize**($\mathcal{G}_j$) # normalize the objectives in $\mathcal{G}_j$
    Associate($\mathcal{G}_j$,$\mathcal{Z}$) #associate each member in $\mathcal{G}_j$ with the reference points
    $\mathcal{G}_j$ = **Preservation**($\mathcal{G}_j$) #choose the new members in the next generation $\mathcal{G}_{j+1}$ based on their niche counts
  $j = j+1$
While $l \le L$: # the algorithm of SA
  $\mathcal{G}_G$ =**Anneal**($\mathcal{G}_G$)# the anneal operation for each member in $\mathcal{G}_G$
  $l = l+1$

grammatical structure, in which **While**, **For** represent the loop structure, **If**, **Else** represent the judgment structure, and the symbol # represents the notes in the procedure of the algorithm.

NSGA3 adopts a ranking method based on reference points instead of the non-dominated ranking between solutions, which can ensure the diversity of Pareto front solutions for subsequent negotiation by airlines.

Firstly, generate the set of reference points based on Das and Dennis's method [40], which is described in Table 8:

TABLE 8. Algorithm for generating the set of reference points.

Algorithm3: **Generate the set of reference points**
Input: the number of the objective functions: M, number of divisions for each objective function: F
Output: the set of reference points $\mathcal{Z}$
Initialize: $\mathcal{Z} = \varnothing$; M = 5; F = 10
For $m \le$ M:
  $x_m = 0 + m$/F
While $x_1 \le 1$:
  $a = x_1$; $b = x_2$; $c = x_3$; $d = x_4$; $e = x_5$
  $s_1 = a$; $s_2 = b - a$; $s_3 = c - b$; $s_4 = d - c$; $s_5 = 1 - e$
  reference point $\boldsymbol{Z} = (s_1, s_2, s_3, s_4, s_5)$
  $\mathcal{Z} = \mathcal{Z} \cup \boldsymbol{Z}$
  $x_1 = x_1 + 1$ / F

The **cross and mutate** function is used to generate the new members, which contributes to the population diversity. Therefore, it is very important to design a mechanism to generate new solutions with high quality. The pseudocode of the **cross and mutate** function is described in Table 9.

TABLE 9. The function of cross and mutate.

Function: **cross and mutate**
Input: the j-th generation set $\mathcal{G}_j$
Output: extra members set q after the mutation of $\mathcal{G}_j$
Hyper-parameters: The mutation rate ε
Initialize: ε = 0.8
For each two members $\boldsymbol{X}_i$ and $\boldsymbol{X}_{i+1}$: # Operation of cross
  If random(0,1) ≤ ε/2 : #function **random** is used to generate a random number in the range of (minimum number, maximum number)
    f_n = **random**($\mathcal{F}$)
    a = **random**(0,**len**($\boldsymbol{P}_{fn}^i$)/2); b = **random**(**len**($\boldsymbol{P}_{fn}^i$)/2,**len**($\boldsymbol{P}_{fn}^i$))
    #function **len** is used to get the number of elements in $\boldsymbol{P}_{fn}$
    $\boldsymbol{P}_{fn}^i$ [a:b] = $\boldsymbol{P}_{fn}^{i+1}$[a:b] #exchange part of waypoints of the same flight
    $\boldsymbol{H}_{fn}^i[a+1{:}b+1] = \boldsymbol{H}_{fn}^{i+1}[a+1{:}b+1]$ # exchange flight levels
    $\boldsymbol{V}_{fn}^i[a+1{:}b+1] = \boldsymbol{V}_{fn}^{i+1}[a+1{:}b+1]$ # exchange speed of the same flight
  Else:
    Continue
For each member $\boldsymbol{X}_i$ in $\mathcal{G}_j$: # Operation of mutate
  If random(0,1) ≤ ε/2 :
    f_n=**random**($\mathcal{F}$); r=**random**($\boldsymbol{A}_{fn}$); p=**random**($\boldsymbol{P}_{fn}$)
    for the p in $\boldsymbol{P}_{fn}$ of the solution $\boldsymbol{X}_i$, p=**random**($\mathcal{P}_p$)
    for the $h_{fn}{}^r$ in $\boldsymbol{H}_{fn}$ of the solution $\boldsymbol{X}_i$, $h_{fn}{}^r = h_{fn}{}^r + 0.6$km, $h_{fn}{}^r \in \mathcal{H}$
  Elif ε/2 < **random**(0,1) ≤ ε :
    f_n=**random**($\mathcal{F}$); r=**random**($\boldsymbol{A}_{fn}$) ; p=**random**($\boldsymbol{P}_{fn}$)
    for the p in $\boldsymbol{P}_{fn}$ of the solution $\boldsymbol{X}_i$, p=**random**($\mathcal{P}_p$)
    for the $h_{fn}{}^r$ in $\boldsymbol{H}_{fn}$ of the solution $\boldsymbol{X}_i$, $h_{fn}{}^r = h_{fn}{}^r$ - 0.6km, $h_{fn}{}^r \in \mathcal{H}$
  Else:
    Continue

The function of **Normalize** is used to map all objective functions to the interval of [0,1]. So we can compare the objective functions of different solutions directly. The pseudocode of the**Normalize** function is shown in Table 10.

The function of **Associate** is used to pair each solution with the reference points generated before. Then these solutions will be ranked and preserved in the following steps. The pseudocode of the **Associate** function is shown in Table 11.

The function of **Preservation** is used to preserve the solutions with good fitness. In order to make the diversity of

TABLE 10. The function of normalize.

Function: **Normalize**
Input: the j-th solution set $\mathcal{GN}$ before normalization
Output: the j-th solution set $\mathcal{GN}$ after normalization
Initialize: m=0
Hyper-parameters: the interval after normalization:[0,1], the number of objectives: M = 5.
While $m \leq$ M :
$maxZ_m$ = **max**($\mathcal{GN}$[Z_m]); $minZ_m$ = **min**($\mathcal{GN}$[Z_m])
For each member $\boldsymbol{X}_i$ in $\mathcal{GN}$:
While $m \leq$ M :
For each Z_m in $\boldsymbol{X}_i$:
$Z'_m = (Z_m - minZ_m) / (maxZ_m - minZ_m)$
$Z_m = Z'_m$

TABLE 11. The function of associate.

Function: **Associate**
Input: the j-th generation set $\mathcal{G}_j$ before associate, reference points set $\mathcal{Z}$
Output: the set $dict[\boldsymbol{Z}]$ after associating with reference points
For each reference point $\boldsymbol{Z}$ in $\mathcal{Z}$:
$dict[\boldsymbol{Z}] = \varnothing$
For each member $\boldsymbol{X}_i$ in $\mathcal{GN}$:
$dict[\boldsymbol{Z}] = dict[\boldsymbol{Z}] \cup$ argmin $_{X_i \in \mathcal{GN}} \{\|\boldsymbol{Z},\boldsymbol{X}_i\|_2\}$

solutions, the preservation operation is based on the ranking of the reference, which is the main difference between NSGA2 and NSGA3. The pseudocode of the **Preservation** function is shown in Table 12:

TABLE 12. The function of preservation.

Function: **Preservation**
Input: the j-th generation set $\mathcal{G}_j$ before preservation, $dict[\boldsymbol{Z}]$
Output: The j-th generation set $\mathcal{G}_j$ after preservation
Hyper-parameters: the scale of generation M
While $\| \mathcal{G}_j \|_0 \geqslant$ M:
For each $\boldsymbol{Z}$ in $dict[\boldsymbol{Z}]$:
Niche($\boldsymbol{Z}$) = $\|dict[\boldsymbol{Z}]\|_0$
$\boldsymbol{Z}$=argmax $_Z$ | **Niche**($\boldsymbol{Z}$) $\|_0$
For each $\boldsymbol{X}_i$ in $dict[\boldsymbol{Z}]$:
$Z_{total}{}^i = Z_1{}^i + Z_2{}^i + Z_3{}^i + Z_4{}^i + Z_5{}^i$ #sum of all of normalized objectives, thus $Z_{total}{}^i$ is the fitness of solution $\boldsymbol{X}_i$
Remove $\boldsymbol{X}_i$ with the worst fitness from $dict[\boldsymbol{Z}]$

The function of **Anneal** is used to optimize the speed of the flights in different flight segments. This function is based on the simulated annealing algorithm [39]. The pseudocode of the **Anneal** function is shown in Table 13.

V. SIMULATION

A. PREDICTION OF FLOW DENSITY

The experiment in this simulation scenario extracted ADS-B trajectory data of all flights in China in November 2019, then counted the hourly flight flow numbers and the total flight time in each airspace. Then calculate the value of flow density in 24-hour of different airspace in November 2019 according to their boundary, the value of flow density obtained in different airspaces in China is shown in Fig. 6 and Fig. 7 (UTC):

TABLE 13. The function of annealing.

Function: **Anneal**
Input: the last generation $\mathcal{G}_G$
Output: the solution $\mathcal{G}_G$ after annealing
Hyper-parameters: step length, T, R, η
Initialize: step length = 0.1, T_s = 1, R = 0.001, η = 0.999
For each member $\boldsymbol{X}_i$ in $\mathcal{G}_G$:
For each $\boldsymbol{x}_{fn}$ in $\boldsymbol{X}_i$: # $\boldsymbol{x}_{fn}$ has been explained in Section III-E
While R $\leq T$:
$\boldsymbol{V}'_I$ = **N**(u=$\boldsymbol{V}_i$, σ=step length) #**N** is the normal distribution function with the mean value u and the variance σ
If $Z'_{total}{}^i \leq Z_{total}{}^i$: # $Z_{total}{}^i$ is the fitness of the solution $\boldsymbol{X}_i$
$\boldsymbol{V}_i = \boldsymbol{V}'_i$
Elif Random(0,1) $\leq T_s$: #Metropolis principle
$\boldsymbol{V}_i = \boldsymbol{V}'_i$
$T = T^{\eta}$

70% of the statistical flow density data is selected randomly as the training data input of the LSTM model, and the remaining 30% of the data is used as the validation data. The flow density prediction model of each airspace is obtained by training the LSTM model in the training data set, and the generalization performance of the prediction model is evaluated in the validation data set. The prediction performance which is reflected by the mean absolute error (MAE) changes with training epochs as shown in Fig. 8. Taking the ZGGGAR05 sector as an example, the comparison between the actual value of flow density and the predicted value of flow density by the LSTM model is shown in Fig. 9.

It can be found from Fig. 9 that the generalization performance of the trained LSTM flow density prediction model is acceptable. MAE reflects the prediction error of the model, and can be calculated by (37):

$$\mathrm{MAE}=\frac{1}{T}\sum_{t=1}^{T}\left|fd_t^{\mathrm{predict}}-fd_{\mathrm{t}}^{\mathrm{true}}\right| \tag{37}$$

In Equation (37), fd_t^{predict} represents the predicted value of flow density, fd_t^{true} is the true value of flow density in historical data, and T is the number of timestamps predicted by the model.

The MAE in the validation data set is about 0.15, and the prediction percentage error is around 3.5%. To further verify its performance, classify the value with a flow density greater than 4 as the peak period, and the value less than or equal to 4 is classified as the normal period. The predicted MAE for these two categories is shown in Table 14:

It can be found that the model does not have the problem of large error in the prediction of the flow density during the peak or trough period (except for some peak values and trough values). After validation, this flow density prediction model can be used for subsequent synergetic trajectory optimization as a module of congestion.

B. ORIGINAL FLIGHT PLANS

The simulation extracted 7 flight plans to arrive in China or depart from China, constructed the optimization model then

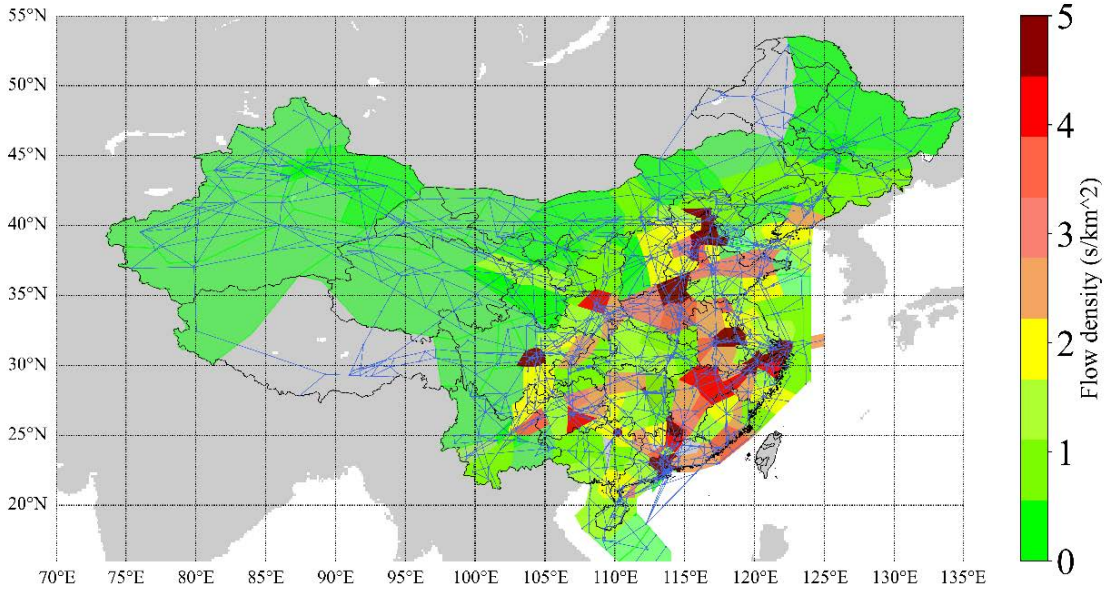

FIGURE 6. The civil airspace structure of China and the distribution of flow density at 00:00, 2019-11-01 (UTC).

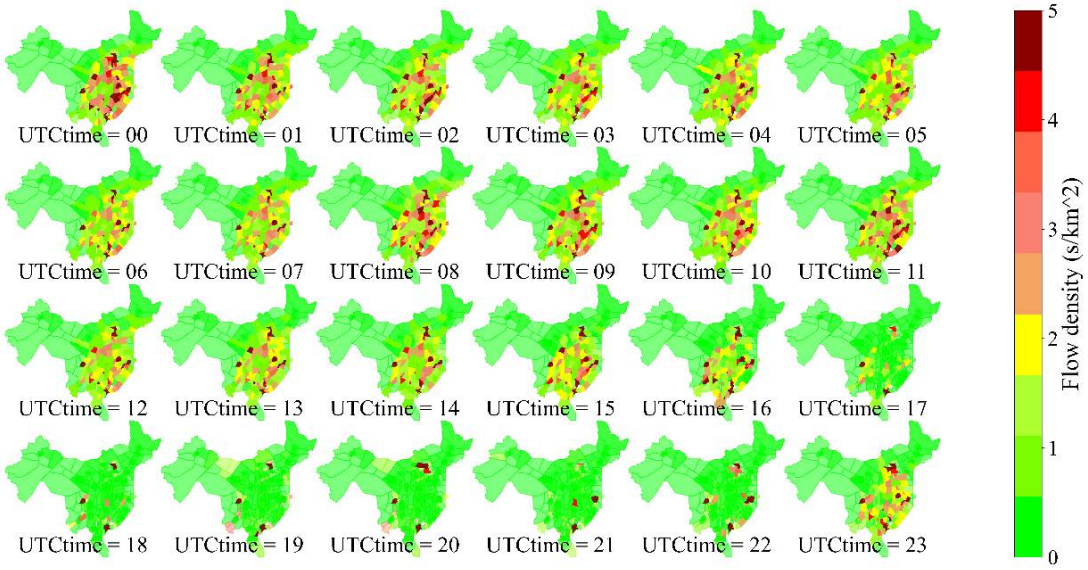

FIGURE 7. The distribution of flow density from 00:00 to 23:00, 2019-11-01 (UTC).

TABLE 14. The MSE of the peak and normal period.

Class	Peak period	Normal period
MAE	0.146	0.166

use the algorithm of NSGA3-SA to solve this optimization problem. The original flight plan includes the information on the aircraft type, air-way points, required time of arrival, speed, and altitude, as shown in Table 15. And the overview of the original flight plan is shown in Fig. 10.

Calculate the flight range, fuel consumption, potential conflicts, congestion, and the difference between RTA and CTA of the original flight plan based on the aircraft dynamics model and the fuel consumption model. The value of these objectives composed by each flight is shown in Table 16.

C. FLIGHT PLANS AFTER OPTIMIZING (SOLUTIONS OF PARETO FRONT)

After building the optimization model of the flight plans, use the algorithm of NSGA3-SA to solve this problem. Because the optimization model and the algorithm of NSGA3-SA

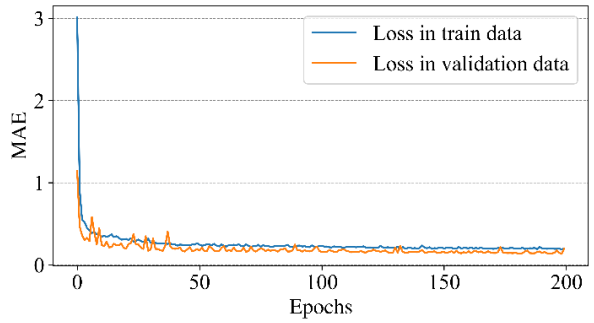

FIGURE 8. The distribution of flow density from 00:00 to 23:00 (UTC).

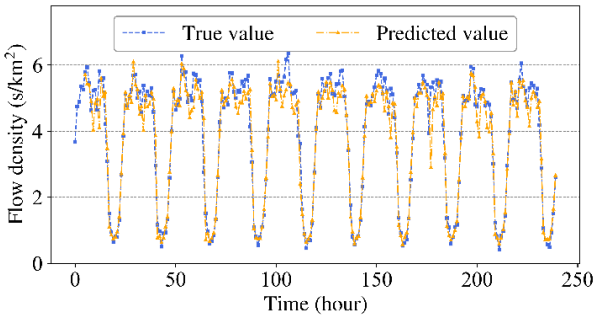

FIGURE 9. The distribution of flow density from 00:00 to 23:00 (UTC).

TABLE 15. One of the original flight plans for optimization.

Type (B747)	Waypoint (lon,lat)	Speed (Mach)	Altitude (QNE, km)	Time (UTC, h:m)
1	BEKOL (114.133,22.543)	0.84	9.8	00:35
2	IDUMA (113.952,22.896)	0.84	9.8	00:37
3	SHL (113.851,23.093)	0.84	9.8	00:39
4	YIN (113.416,24.192)	0.84	9.8	00:47
…	…			
49	NIRAV (88.984,45.878)	0.84	9.8	04:56
50	TAI (88.085,47.748)	0.84	9.8	04:48
51	GOPTO (87.467,49.092)	--	--	04:56

PS: TABLE XV is just part of the original flight plans due to the limitation of the paper.

including the hypermeters setting for the algorithm have been described in Section III and Section IV, the content in this section is mainly about the solution analysis of this optimization problem.

Firstly, part of the Pareto optimal frontiers solution obtained by the NSGA3-SA and their normalized objectives value is given below, which is shown in Fig. 11.

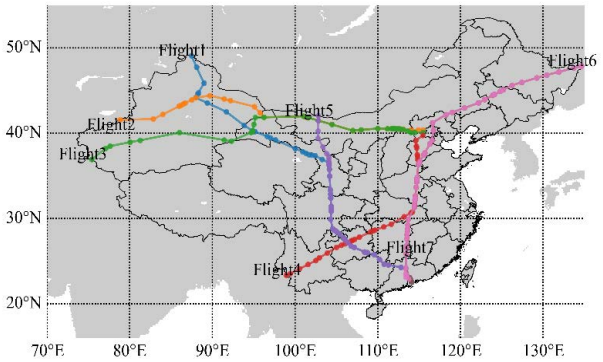

FIGURE 10. The outline of the original flight plan.

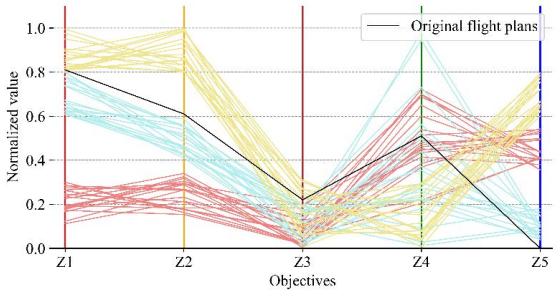

FIGURE 11. Part of the solutions in the Pareto front of NSGA3-SA.

In Fig. 11, each line represents the objective value of a feasible solution in the Pareto front. The lower the normalized value of each objective (Z1-Z5) is, the better this feasible solution is. The process of normalization is:

$$Z_i = \frac{Z_i - \min(Z_i)}{\max(Z_i) - \min(Z_i)}, i \in \{1, 2, \ldots, 5\}, Z_i \in Z_{\text{front}} \tag{38}$$

In Equation (38), Z_i is the value of objectives that represents the fuel consumption, flight range, and other attributes of the flights (Section III-E). $\mathbf{Z}_{\text{front}}$ represents the solutions in the Pareto front and Z_i is the value of objectives after the process of normalization, which is the value plotted in Fig. 11.

The authors denote solutions with analogous objective functions with the same color for visualization. The black lines in Fig. 11 represent the normalized objective function values of the original flight plan. This type of figure is used to show the numerical value of the objective function corresponding to the optimal solution when the number of objective functions is more than three.

It can be found in Fig. 11 that the objectives of the flight range (Z1), fuel consumption (Z2), potential conflicts (Z3), and congestion (Z4) of the Pareto front solutions could have a better value compared to the original flight plans. To avoid the optimized flight plan having changed too much compared to the original flight plan, the target Z5 is used to limit the changing extent of the flight plan [41]. It can be found that as long as the RTA of the flight plans is properly adjusted

TABLE 16. The objectives' value of the original flight plans.

Flight (type)	Flight range (km)	Fuel consumption (kg)	Potential conflicts	Congestion (s/km^2)	Difference between RTA and CTA (min)
Flight1 (B747)	4326	75440	0	46.69	0
Flight2 (B747)	3250	51754	3	7.83	0
Flight3 (A330)	3740	68581	0	9.18	0
Flight4 (B747)	2763	47479	2	52.40	0
Flight5 (A330)	2561	43253	1	29.23	0
Flight6 (A330)	3754	65042	4	68.70	0
Flight7 (B747)	3720	65944	4	83.26	0
Total	24114	417498	14	297.30	0

TABLE 17. The objectives' value of the optimized flight plans.

Flight (type)	Flight range (km)	Fuel consumption (kg)	Potential conflicts	Congestion (s/km^2)	Difference between RTA and CTA (min)
Flight1 (B747)	4243	71454	0	46.55	0.4
Flight2 (B747)	3231	51754	0	7.57	0.2
Flight3 (A330)	3622	65005	0	9.14	0.3
Flight4 (B747)	2763	42697	0	51.40	2.3
Flight5 (A330)	2560	43253	0	27.23	1.5
Flight6 (A330)	3754	61627	0	62.70	3.1
Flight7 (B747)	3720	62505	0	81.26	2.6
Total	23894	398298	0	285	10.4

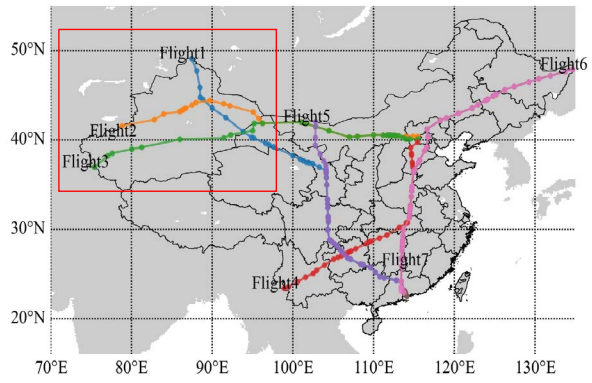

FIGURE 12. The outline of the optimized flight plan.

(even without adjusting the RTA just to adjust the speed of the flight, as the blue lines in Fig. 11), the flight plan could have better benefits in the objectives of flight range (Z1), fuel consumption (Z2), potential conflict (Z3), and congestion (Z4).

One of the solution's objectives in the Pareto front is shown in Table 17 (one of the solutions in the red line in Fig. 11). And the overview of the flight plan after optimization is shown in Fig. 12.

It can be found from Table 17 that the value of the objectives including the flight range, fuel consumption, potential conflicts, and congestion is better than the original flight plans. The main difference between the selection of waypoints before optimized flight plans is in northwest China (The red box in Fig. 12) compared to Fig. 10. There are lots of sparse routes in northwest China, which provides extra waypoint options for flight planning. So it can be considered that the algorithm makes a good trajectory optimization effect by searching the better solutions.

VI. ANALYSIS OF ALGORITHM

A. COMPARISON OF SOLUTIONS BY DIFFERENT ALGORITHMS IN SIMULATION SCENARIO

In order to analyze the performance of the NSGA3-SA algorithm furtherly, the NSGA2 [41], NSGA3 [35], and NSGA2-SA algorithms are used to optimize the flight plans in the simulation scenario above.

For NSGA2 and NSGA3, the principle of the non-dominated judgment of solutions, the steps of generating the reference points, sorting based on the reference points, and cross-mutating in the population are the same as described in Section IV. Finally, the NSGA2-SA algorithm has the same technical route as NSGA3-SA, which search for non-dominated Pareto fronts for further optimization by using the simulated annealing algorithm. The pseudo-code of the NSGA2-SA algorithm is as Table 18.

NSGA2 selects the members based on the non-dominated sorting rather than sorting based on the reference points, so there are some differences in algorithm initialization and the process of member sorting between NSGA2 and NSGA3. The function of Non-dominated sorting is shown in Table 19.

TABLE 18. The algorithm pseudocode of NSGA2-SA.

Algorithm2: **NSGA2-SA**
Input: parent generation set $\mathcal{G}_0$
Output: the last generation $\mathcal{G}_G$ of solutions (Pareto front solutions)
Hyper-parameters: G, K, L
While $j \leq$ G:# the algorithm of NSGA2
  $\mathcal{GN} = \mathcal{G}_j$
  While $k \leq K$:
    $g = \mathcal{GN}$
    q = **Cross and mutate**(g) #the recombination and mutation operation for g
    $\mathcal{GN} \cup q$
    $K = k+1$
  $\mathcal{G}_j = \mathcal{GN}$
  $\mathcal{G}_j$ = **Normalize**($\mathcal{G}_j$) # normalize the objectives in $\mathcal{G}_j$
  Non-dominated sorting($\mathcal{G}_j$) #non-dominated sorting is the sorting method of NSGA2
  If $\|\mathcal{GN}\|_0 = \|\mathcal{G}_j\|_0$:
    $\mathcal{G}_j = \mathcal{G}_j$, **Break to** the algorithm of SA
While $l \leq L$: # the algorithm of SA
  $\mathcal{G}_G$ =**Anneal**($\mathcal{G}_G$)# the anneal operation for each member in $\mathcal{G}_G$
  $l = l+1$

TABLE 19. The function of non-dominated sorting.

Function: **Non-dominated sorting**
Input: the j-th generation set $\mathcal{G}_j$ before non-dominated sorting
Output: The j-th generation set $\mathcal{G}_j$ after non-dominated sorting
Hyper-parameters: the scale of generation M
Initialize: $\mathcal{G}_{j+1} = \emptyset$
Calculate the objection function Z_1- Z_5 for each number in $\mathcal{G}_j$
For each member $\boldsymbol{X}_i$ in $\mathcal{G}_j$:
  For each member $\boldsymbol{X}_k$ in $\mathcal{G}_j$:
    If any Z_1- Z_5 of $\boldsymbol{X}_i \leq Z_1$- Z_5 of $\boldsymbol{X}_k$
      Continue
    Else:
      $Z_{total}^{\ i} = Z_1^{\ i} + Z_2^{\ i} + Z_3^{\ i} + Z_4^{\ i} + Z_5^{\ i}$ #sum of all of normalized objectives, thus $Z_{total}^{\ i}$ is the fitness of solution $\boldsymbol{X}_i$
      Break
  $\mathcal{G}_{j+1} \cup \boldsymbol{X}_i$
  Remove $\boldsymbol{X}_i$ from $\mathcal{G}_j$
While $\|\mathcal{G}_{j+1}\|_0 \leq$ M:
  $\mathcal{G}_{j+1} \cup \text{argmin}_{X_i} Z_{total}^{\ i}$
  Remove $\boldsymbol{X}_i$ from $\mathcal{G}_j$

1) NSGA2 IN THE SIMULATION SCENARIO

The simulation scenario is the same as Section V, we use NSGA2 to solve this problem of the multi-flight 4D trajectory optimization. Part of the Pareto optimal frontiers solution obtained by the NSGA2 and their normalized objectives value is given below, which is shown in Fig. 13.

It can be found from Fig. 13 that the solutions in the Pareto optimal frontier obtained by NSGA2 are more intense compared with the objectives' value of the red line in Fig. 11. The sorting method of non-dominated ranking of the NSGA2 algorithm is more stringent than the reference point-based ranking, thus leaving the characteristics of the solution individuals more similar. This phenomenon is unfavorable for airline synergetic decision-making because the same class of solutions with similar characteristics are given by the algorithm leaving less room for choice by airlines.

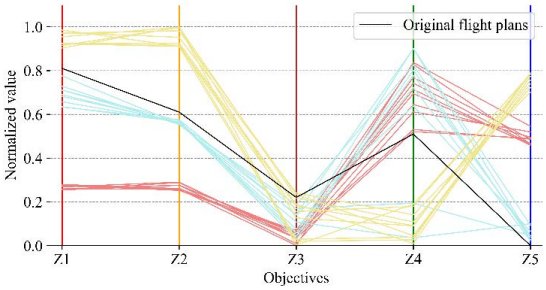

FIGURE 13. Part of the solutions in the Pareto front of NSGA2.

2) NSGA2-SA IN THE SIMULATION SCENARIO

Part of the Pareto optimal frontiers solution obtained by the NSGA2 and their normalized objectives value is given below, which is shown in Fig. 14.

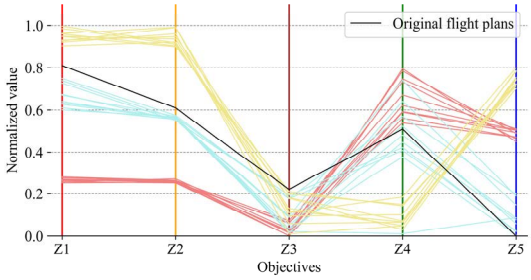

FIGURE 14. Part of the solutions in the Pareto front of NSGA2-SA.

It can be found from Fig. 14 that the solutions in the Pareto optimal frontier obtained by NSGA2-SA are better (it can be observed significantly by the value of Z3 and Z4) compared with the objectives' value Pareto optimal frontier obtained by NSGA2 in Fig. 13. The comparison between NSGA2 and NSGA2-SA can preliminary show the optimization significance of adding the simulated annealing algorithm in this simulation scenario.

3) NSGA3 IN THE SIMULATION SCENARIO

A set of Pareto optimal frontiers obtained by the NSGA3 algorithm after normalization is given below (compared with the objectives' value of the red line in Fig. 11), which is shown in Fig. 15.

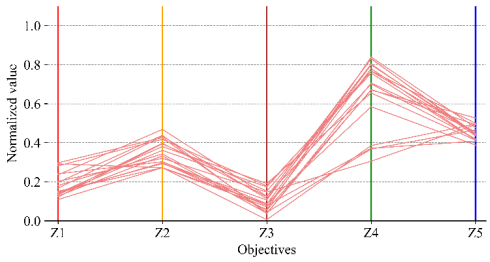

FIGURE 15. Part of the solutions in the Pareto front of NSGA3.

It can be found from Fig. 15 that NSGA3 has a good optimization effect on the flight plan, but the optimization effect on fuel consumption is not ideal. The reason is that cross and mutates operations of the genetic algorithm can reduce the possibility of the population falling into the local optimum, but at the same time, the searchability for the local optimum solution is reduced relatively. Therefore, for continuous variables such as aircraft speed, the cross-mutation operation does not show its advantages. It also explains why the NSGA3-SA algorithm incorporating the search principle of the annealing algorithm is better than the NSGA3 algorithm on the optimal solution frontier.

B. ANALYSIS OF ALGORITHM

1) ANALYSIS OF ALGORITHM SOLUTION PERFORMANCE

To further illustrate the performance of NSGA3-SA and other algorithms for comparison, we choose the harmonic value of the optimal solution (HVOS), inverted generational distance (IGD), and minimum Pareto front error (MPFE) as the performance indicators for these algorithms.

The index of HVOS [42], [43] is used to measure the ability of the algorithm to search for the global optimal solution. The smaller the value of HVOS, the better the global optimal solution obtained by the algorithm. HVOS can be calculated by (39).

$$\mathrm{HVOS} = \frac{\mathrm{R}}{\sum_{i=1}^{\mathrm{R}} Z_i}, Z_i \in [0, 1], \mathrm{R} = 5 \tag{39}$$

In Equation (39), R represents the number of objectives and Z_i is the normalized value of objective function Z_i.

The index of IGD [44] reflects the degree of population convergence and the diversity of solutions in the population. The smaller the IGD, the more single type of solutions in the population. The IGD can be calculated by (40):

$$\mathrm{IGD} = \frac{1}{|Z_{\mathrm{front}}|} \sum_{i=1}^{|Z_{\mathrm{front}}|} \min_{j=1}^{|G|} \left\| z_i, a_j \right\|, z_i \in Z_{\mathrm{front}} \tag{40}$$

In Equation (40), $\boldsymbol{Z}_{\mathrm{front}}$ represents the solutions in the Pareto front, thus $|\boldsymbol{Z}_{\mathrm{front}}|$ is the number of solutions in the Pareto front obtained by the algorithm. $\boldsymbol{G}$ represents all of the solutions in the last generation. a_j is one of the solutions in generation $\boldsymbol{G}$, and z_i is one of the solutions in $\boldsymbol{Z}_{\mathrm{front}}$.

Finally, the index of MPFE [44], [45] is used to reflect the distance of the non-dominated solution set to the Pareto frontier. Usually, the smaller the MPFE is, the better the non-dominated solution is. MPFE can be calculated by (41):

$$\mathrm{MPFE} = \min \left(\left\| \mathrm{Z}(z_i), Z_{\mathrm{opt}} \right\|_2 \right), z_i \in Z_{\mathrm{front}} \tag{41}$$

In Equation (41), z_i is one of the solutions in $\boldsymbol{Z}_{\mathrm{front}}$, $\mathrm{Z}(z_i)$ is the function to get the objectives value of z_i, and $\boldsymbol{Z}_{\mathrm{opt}}$ is the value of the optimal objectives in all of the feasible solutions, which is constructed by $[\mathrm{Z1}_{\min}, \mathrm{Z2}_{\min}, \ldots, \mathrm{Z5}_{\min}]$ in the simulation.

TABLE 20. The indicators of different algorithms in simulation.

Methods	NSGA3-SA	NSGA2-SA	NSGA2	NSGA3
HVOS	1.894	1.894	2.095	2.115
IGD	0.306	0.195	0.204	0.312
MPFE	1.422	1.422	1.688	1.720

Table 20 gives the above indicators' value of different algorithms in this simulation scenario.

It can be found from Table 20 that the ability of NSGA2 and NSGA3 to find the optimum feasible solution is close. But the algorithm of NSGA3 is inclined to preserve more different types of solutions compared to NSGA2, which is a good characteristic because flight plans are required to negotiate by many departments. Compared NSGA2 with NSGA2-SA, and NSGA3 with NSGA3-SA, it can be found that the process of simulated annealing plays a role in optimizing the Pareto front solutions because of the detailed local search of flight speeds by the simulated annealing algorithm.

2) ANALYSIS OF ALGORITHM COMPUTATIONAL COMPLEXITY

Take the above simulation experiment scenario as an example, the running time of those different algorithms is obtained. And the Computational time complexity of NSGA3-SA, NSGA2, and NSGA3 is analyzed in Table 21 [35], [41].

TABLE 21. The complexity of different algorithms.

Methods	NSGA3-SA	NSGA 2-SA	NSGA2	NSGA3
Algorithmic complexity	$\boldsymbol{O}(\mathrm{R}^2\log_{\mathrm{MR}\text{-}2^{\mathrm{R}}} + \mathrm{M})$	$\boldsymbol{O}(\mathrm{MR}^2 + \mathrm{M})$	$\boldsymbol{O}(\mathrm{MR}^2)$	$\boldsymbol{O}(\mathrm{R}^2\log_{\mathrm{M}\text{-}2^{\mathrm{R}}})$
Running time (s)	588	519	365	324

In Table 19, M is the number of populations in each generation, R is the number of objective functions, and $\boldsymbol{O}$ represents the maximum number of operations for a single algorithm iteration.

Since NSGA3-SA uses the genetic algorithm to complete the first search and then uses the simulated annealing algorithm to perform the second search, this algorithm with the process of SA will inevitably have a higher computational complexity than NSGA2 and NSGA3 (the algorithm complexity of the simulated annealing algorithm is $\boldsymbol{O}(\mathrm{M})$). But the running time of this algorithm is still within the acceptable range.

These simulations experimented on a computer with Windows 10, a 64-bit operating system with RAM of 8GB and a CPU of i7-6700. Simulation software is Spyder4 with Python3.8, which mainly concludes the environment of keras2.3.1, tensorflow2.2.0, matplotlib3.2.2, numpy1.18.5, pandas1.2.4, basemap1.2.2. The runtime of the collaborative trajectory planning procedure in Table 21 is obtained in this

environment. In addition, since Python is an execution language based on interpretation, its program running speed is lower than that of machine language or other compiled execution languages. If the program can be executed in machine language or compiled language, the execution speed of this algorithm would have great room for improvement.

C. ALGORITHM APPLICABILITY AND PERFORMANCE IN COMMON TRAJECTORY PLANNING PROBLEMS

From the perspective of algorithm initialization and iteration, the NSGA3-SA algorithm has advantages for many objectives, mixed-integer nonlinear problems (MINLP) with both discrete and continuous decision variables, such as synergetic 4D trajectory planning for flights. In order to verify the universality of the NSGA3-SA algorithm in trajectory planning problems, we add three simpler but universal scenarios as supplementary experiments to further demonstrate the performance of the algorithm.

1) SCENARIO1: SYNERGETIC FLIGHT PLAN MULTI-OBJECTIVE OPTIMIZATION WITHOUT CONSIDERING AIRSPACE CONGESTION

Then we discuss the application of the NSGA3-SA algorithm in a relatively simple scenario: synergetic flight plan multi-objective optimization without considering airspace congestion. This scenario is generally the same as Section V (Fig. 10), which does not consider reducing airspace congestion (objective Z4). Scenario1 considers only the flight range (Z1), fuel consumption (Z2), potential conflicts (Z3), and aircraft punctuality (Z5) objectives for flight trajectory planning (Scenario1 is similar to the scenario in Reference [46]). A set of Pareto optimal frontiers obtained by the NSGA3-SA algorithm after normalization is given in Fig. 16.

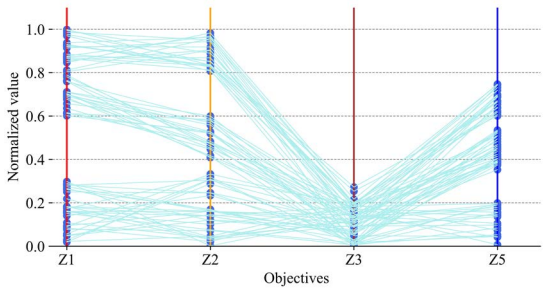

FIGURE 16. Part of the Pareto front solutions of NSGA3-SA in Scenario1.

NSGA2, NSGA3, and NSGA2-SA algorithms are used for comparative experiments in the Scenario1. The performance indicators of different algorithms are shown in Table 22 below:

It can be found from Table 22 that NSGA3-SA can be applied to Scrnario1: Synergetic flight plan multi-objective optimization without considering airspace congestion. Moreover, compared with several other algorithms, the NSGA3-SA algorithm still retains the advantages of high computational efficiency and obvious differences between the non-dominated optimal solutions.

TABLE 22. The indicators of different algorithms in scenario1.

Methods	NSGA3-SA	NSGA2-SA	NSGA2	NSGA3
HVOS	1.213	1.268	1.555	1.467
IGD	0.288	0.136	0.141	0.291
MPFE	0.768	0.815	1.047	0.953
Running Time (s)	421	417	264	252

2) SCENARIO2: MULTI-OBJECTIVE OPTIMIZATION FOR SINGLE AIRCRAFT TRAJECTORY

We use a flight plan of a B737-800 from Guangzhou to Urumqi, China as Scenario2. The trajectory of this flight is shown in Fig. 17. This is a scenario of multi-objective optimization for a single aircraft trajectory. We do not consider the problem of synergetic optimization of multiple flights and the resolution of conflicts between flights in Scenario2 but consider only the objectives of flight range (Z1), fuel consumption (Z2), congestion (Z4), and aircraft punctuality (Z5) for flight trajectory planning (this scenario is similar to the scenario in Reference [47]). A set of Pareto optimal frontiers obtained by the NSGA3-SA algorithm after normalization is given in Fig. 18.

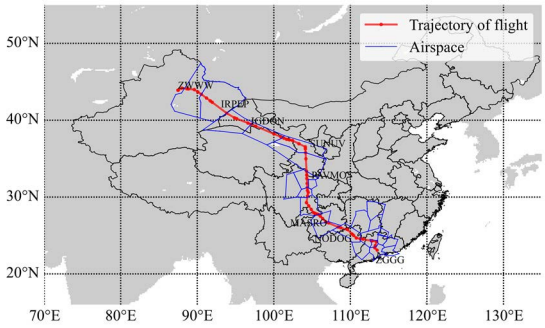

FIGURE 17. The outline of the flight plan in Scenario2.

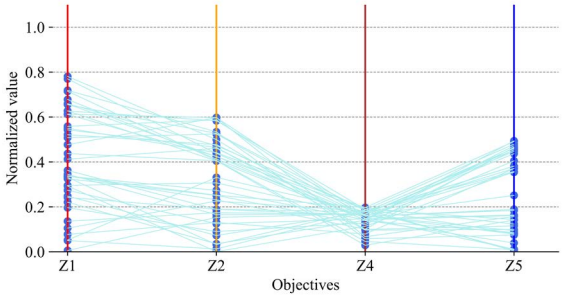

FIGURE 18. Part of the Pareto front solutions of NSGA3-SA in Scenario2.

NSGA2, NSGA3, and NSGA2-SA algorithms are used for comparative experiments in Scenario2. The performance indicators of different algorithms are shown in Table 23:

TABLE 23. The indicators of different algorithms in scenario2.

Methods	NSGA3-SA	NSGA2-SA	NSGA2	NSGA3
HVOS	1.426	1.425	1.557	1.557
IGD	0.262	0.128	0.137	0.314
MPFE	0.818	0.819	1.115	1.111
Running Time (s)	195	201	102	121

It can be found that NSGA3-SA can be applied to Scrnario2: multi-objective optimization for a single aircraft trajectory. However, the algorithmic superiority of NSGA3-SA does not have much advantage over NSGA2 or NSGA3 in Scenario2. With the simplification of the problem, the search space of the decision variables becomes smaller, and both four algorithms can meet the searching needs well. The solution results and the running time of NSGA2 and NSGA3 in Scenario2 are close to the performance shown in experiments by other scholars [39], [44].

3) SCENARIO3: DUAL-OBJECTIVE TRAJECTORY OPTIMIZATION CONSIDERING THE FUEL CONSUMPTION AND CONTROL TIME OF ARRIVAL

We use a flight plan of a B737-800 from Guangzhou to Urumqi, China as Scenario3, and the trajectory of the flight is shown in Figure 17 too. Scenario3 is an optimization problem for a single aircraft trajectory with two objectives: minimum fuel consumption and the running time of the flight (this scenario is similar to the scenario in Reference [48]). A set of Pareto optimal frontiers obtained by the NSGA3-SA algorithm of this scenario is shown in Fig.19.

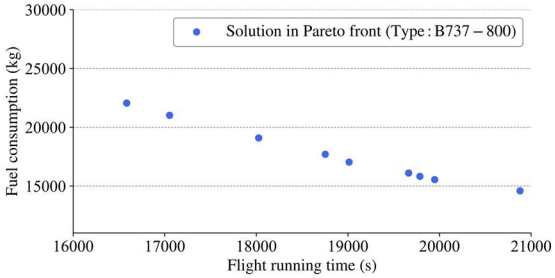

FIGURE 19. Part of the Pareto front solutions of NSGA3-SA in scenario3.

NSGA2, NSGA3, and NSGA2-SA algorithms are used for comparative experiments in Scenario3. The performance indicators of different algorithms are shown in Table 24 below:

It can be found that the NSGA3-SA algorithm is still applicable in Scenario3, but its solution performance does not show a great advantage compared with the NSGA2 and NSGA3 algorithms. NSGA3-SA and NSGA2-SA take a lot of computing time but do not obtain a non-dominated optimal solution with obvious quality improvement. If the airline wants to further optimize the flight plan of a certain flight

TABLE 24. The indicators of different algorithms in scenario3.

Methods	NSGA3-SA	NSGA2-SA	NSGA2	NSGA3
HVOS	0.722	0.727	0.727	0.729
IGD	0.243	0.183	0.189	0.246
MPFE	0.445	0.483	0.491	0.489
Running Time (s)	81	79	42	50

or wants to obtain some flight plans relatively novel, then the NSGA3 and NSGA3-SA algorithms are good choices.

It can be seen from the three scenarios above that the NSGA3-SA algorithm shows good applicability for the problem of 4D trajectory optimization. The more decision variables, the larger the search space, and the more objective functions in the synergetic trajectory planning problem, the advantages of NGSA3-SA will be more significant theoretically. In addition, the NSGA3-SA algorithm can retain some non-dominated solutions with obvious differences, rather than retain the similar or same type of optimal solutions in many-objectives optimization like NSGA2. This attribute of NSGA3-SA (this feature comes from NSGA3) means airlines or related departments can have more kinds of different choices.

VII. CONCLUSION

The following are the main conclusions and analyses of both the advantages and disadvantages of this paper:

(1) For the pre-tactical synergetic trajectory planning problem, the algorithm of NSGA3-SA has the advantage of searching for the optimal solution for many objectives while keeping the complexity of this algorithm within an acceptable range. At the same time, the Pareto frontier solutions obtained by this algorithm have better values of objectives while maintaining the diversity of solutions.

(2) There is little coordination between different airlines in the production of flight plans in many countries at present. Therefore, small-scale synergetic trajectory optimization can be used to balance airspace conflicts and improve the efficiency of flights. It can be found from the simulations that there is some room for optimization in the flight plans for most of the current flights.

(3) With the development of TBO, the information sharing among airports, air traffic management departments, and airlines will be strengthened, and the flight scale of synergetic trajectory planning will become larger. The synergetic trajectory planning model and its algorithm proposed in this paper have the characteristics of universal applicability, and good reproducibility, which can be applied to large-scale synergetic trajectory planning.

While acknowledging the value of the model and algorithm in this paper, we should not neglect two main limitations of the algorithm in large-scale synergetic trajectory planning:

(1) The more aircraft involved in synergetic trajectory planning, the more difficult it is to negotiate between airlines,

and it is difficult to make all users satisfied with the final selection of the solution in the Pareto frontier given by the algorithm.

(2) When the number of flights for synergetic trajectory planning exceeds a certain number, the impact of the planned aircraft on airspace congestion should not be ignored. Large-scale synergetic trajectory planning may cause the congestion prediction model to lose its good prediction performance because of the impact of the flights planned by the optimization model and algorithm.

ACKNOWLEDGMENT

Author Contributions: Jinlun Zhou: built the models, conducted the analysis, interpreted the results, and wrote the manuscript of this research; Honghai Zhang: designed the study and contributed to the background of this research; Yufei Wang: contributed to the algorithm design, simulations, and experiments for this research; Gang Zhong: helped to construct the trajectory planning model and the congestion prediction model; and Hao Liu: checked the model and helped to design the algorithm.

REFERENCES

[1] S. Ruiz, L. Guichard, N. Pilon, and K. Delcourte, "A new air traffic flow management user-driven prioritisation process for low volume operator in constraint: Simulations and results," *J. Adv. Transp.*, vol. 2019, pp. 1–21, Apr. 2019.

[2] A. Harada, T. Ezaki, T. Wakayama, and K. Oka, "Air traffic efficiency analysis of airliner scheduled flights using collaborative actions for renovation of air traffic systems open data," *J. Adv. Transp.*, vol. 2018, no. 1, pp. 1–22, Jun. 2018.

[3] M. B. Ahmed, W. Ghroubi, M. Haouari, and H. D. Sherali, "A hybrid optimization-simulation approach for robust weekly aircraft routing and retiming," *Transp. Res. C, Emerg. Technol.*, vol. 84, pp. 1–20, Nov. 2017.

[4] H. Xie, Z. Li, and F. Liu, "Research on the optimization of the four-dimensional trajectory of city pair under capacity limitation," *Acta Aeronautica et Astronautica Sinica*, vol. 42, pp. 1–20, Feb. 2021.

[5] H. G. Visser and R. A. A. Wijnen, "Optimization of noise abatement departure trajectories," *J. Aircr.*, vol. 38, no. 4, pp. 620–627, Jul. 2001.

[6] J. Wan, H. Zhang, F. Liu, and W. Lyu, "Optimization of aircraft climb trajectory considering environment impact under RTA constraints," *J. Adv. Transp.*, vol. 2020, pp. 1–20, Aug. 2020.

[7] X. Prats, V. Puig, J. Quevedo, and F. Nejjari, "Multi-objective optimisation for aircraft departure trajectories minimising noise annoyance," *Transp. Res. C, Emerg. Technol.*, vol. 18, no. 6, pp. 975–989, Dec. 2010.

[8] R. Torres, J. Chaptal, C. Bès, and J.-B. Hiriart-Urruty, "Optimal, environmentally friendly departure procedures for civil aircraft," *J. Aircr.*, vol. 48, no. 1, pp. 11–22, Jan. 2011.

[9] V. Ho-Huu, S. Hartjes, H. Visser, and R. Curran, "An efficient application of the MOEA/D algorithm for designing noise abatement departure trajectories," *Aerospace*, vol. 4, no. 4, p. 54, Nov. 2017.

[10] R. Gu, J. Yuan, X. Han, Z. Wei, and N. Li, "Flight performance optimization considering environmental impact under multi-RTA constraints," *Int. J. Aeronaut. Space Sci.*, vol. 20, no. 4, pp. 964–977, Dec. 2019.

[11] F. Li and Z. Li, "Research on rapid planning of intelligent aircraft trajectory under multiple constraints," *J. Phys., Conf.*, vol. 1592, no. 1, Aug. 2020, Art. no. 012021, doi: 10.1088/1742-6596/1592/1/012021.

[12] X. Qian, J. Mao, C.-H. Chen, S. Chen, and C. Yang, "Coordinated multi-aircraft 4D trajectories planning considering buffer safety distance and fuel consumption optimization via pure-strategy game," *Transp. Res. C, Emerg. Technol.*, vol. 81, pp. 18–35, Aug. 2017.

[13] D. B. Seenivasan, A. Olivares, and E. Staffetti, "Multi-aircraft optimal 4D online trajectory planning in the presence of a multi-cell storm in development," *Transp. Res. Part C: Emerg. Technol.*, vol. 110, pp. 123–142, Jan. 2020.

[14] A. Gardi, R. Sabatini, and T. Kistan, "Multiobjective 4D trajectory optimization for integrated avionics and air traffic management systems," *IEEE Trans. Aerosp. Electron. Syst.*, vol. 55, no. 1, pp. 170–181, Feb. 2019.

[15] S. Chaimatanan, D. Delahaye, and M. Mongeau, "A hybrid metaheuristic optimization algorithm for strategic planning of 4D aircraft trajectories at the continental scale," *IEEE Comput. Intell. Mag.*, vol. 9, no. 4, pp. 46–61, Nov. 2014.

[16] Y. Xu and X. Prats, "Effects of linear holding for reducing additional flight delays without extra fuel consumption," *Transp. Res. D, Transp. Environ.*, vol. 53, pp. 388–397, Jun. 2017.

[17] Y. Tian, X. He, Y. Xu, L. Wan, and B. Ye, "4D trajectory optimization of commercial flight for green civil aviation," *IEEE Access*, vol. 8, pp. 62815–62829, 2020.

[18] H. G. Visser and S. Hartjes, "Economic and environmental optimization of flight trajectories connecting a city-pair," *Proc. Inst. Mech. Eng., G, J. Aerosp. Eng.*, vol. 228, no. 6, pp. 980–993, May 2014.

[19] S. Solak and H. Chen, "Optimal metering point configurations for optimized profile descent based arrival operations at airports," *Transp. Sci.*, vol. 52, no. 1, pp. 150–170, Jan. 2018.

[20] M. Soler, B. Zou, and M. Hansen, "Flight trajectory design in the presence of contrails: Application of a multiphase mixed-integer optimal control approach," *Transp. Res. C, Emerg. Technol.*, vol. 48, pp. 172–194, Nov. 2014.

[21] L. Yang, W. Li, F. Liu, Y. Chen, and Z. Zhao, "Multi-objective optimization of continuous descending trajectories in flexible airspace," *Acta Aeronautica et Astronautica Sinica*, vol. 42, no. 2, Sep. 2021, Art. no. 324157.

[22] A. W. A. Hammad, D. Rey, A. Bu-Qammaz, H. Grzybowska, and A. Akbarnezhad, "Mathematical optimization in enhancing the sustainability of aircraft trajectory: A review," *Int. J. Sustain. Transp.*, vol. 14, no. 6, pp. 413–436, Apr. 2019.

[23] Y. Lim, A. Gardi, R. Sabatini, K. Ranasinghe, N. Ezer, K. Rodgers, and D. Salluce, "Optimal energy-based 4D guidance and control for terminal descent operations," *Aerosp. Sci. Technol.*, vol. 95, Dec. 2019, Art. no. 105436.

[24] S. G. Park and J.-P. Clarke, "Optimal control based vertical trajectory determination for continuous descent arrival procedures," *J. Aircr.*, vol. 52, no. 5, pp. 1469–1480, Sep. 2015.

[25] K.-Q. Cai, Y.-W. Tang, and W. Wang, "An evolutionary multi-objective approach for network-wide conflict-free flight trajectories planning," in *Proc. IEEE/AIAA 34th Digit. Avionics Syst. Conf. (DASC)*, Sep. 2015, pp. 1–10.

[26] W. Zeng, X. Chu, Z. Xu, Y. Liu, and Z. Quan, "Aircraft 4D trajectory prediction in civil aviation: A review," *Aerospace*, vol. 9, no. 2, p. 91, Feb. 2022.

[27] L. Ma and S. Tian, "A hybrid CNN-LSTM model for aircraft 4D trajectory prediction," *IEEE Access*, vol. 8, pp. 134668–134680, 2020.

[28] Z. Shi, M. Xu, Q. Pan, B. Yan, and H. Zhang, "LSTM-based flight trajectory prediction," in *Proc. Int. Joint Conf. Neural Netw. (IJCNN)*, Jul. 2018, pp. 1–8.

[29] X. Wu, H. Yang, H. Chen, Q. Hu, and H. Hu, "Long-term 4D trajectory prediction using generative adversarial networks," *Transp. Res. Part C: Emerg. Technol.*, vol. 136, Mar. 2022, Art. no. 103554.

[30] Y. Tian, *Aircraft Performance Engineering*, vol. 4. Beijing, China: Science Press, 2015, pp. 187–214.

[31] *User Manual for the Base of Aircraft Data (BADA)*. Accessed: Feb. 18, 2019. [Online]. Available: https://www.eurocontrol.int/publication/user-manual-base-aircraftdata-bada-revision-37

[32] *Chinese Civil Aviation Regulations Part 71: Measures for the use of Airspace by Civil Aviation*, Civil Aviation Admin. China, Beijing, China, 2004.

[33] W. Lyu, H. Zhang, J. Wan, and L. Yang, "Research on safety prediction of sector traffic operation based on a long short term memory model," *Appl. Sci.*, vol. 11, no. 11, p. 5141, Jun. 2021.

[34] L. Lin, W. Li, and H. Bi, "Vehicle trajectory prediction using LSTMs with spatial-temporal attention mechanisms," *IEEE Intell. Transp. Syst. Mag.*, vol. 14, no. 2, pp. 197–208, Feb. 2021.

[35] D. Kalyanmoy and J. Himanshu, "An evolutionary many-objective optimization algorithm using reference-point-based nondominated sorting approach," *IEEE Trans. Evol. Comput.*, vol. 18, no. 4, pp. 577–600, Sep. 2014.

[36] J. K. Cochran, S.-M. Horng, and J. W. Fowler, "A multi-population genetic algorithm to solve multi-objective scheduling problems for parallel machines," *Comput. Oper. Res.*, vol. 30, no. 7, pp. 1087–1102,Jun. 2003.

[37] C. M. Andreas, *Introduction to Machine Learning With Python*. Beijing, China: Posts Telecom Press, 2018, pp. 212–251.
[38] C. Albon, *Machine Learning With Python Cookbook*. Beijing, China: Publishing House of Electrons Industry, 2019, pp. 147–214.
[39] J. García, M. Soler, and F. J. Saez, "Collocation methods to minimum fuel trajectory problems with required time of arrival in ATM," *J. Aerosp. Inf. Syst.*, vol. 13, no. 7, pp. 243–264, Jun. 2016.
[40] E. Zitzler, K. Deb, and L. Thiele, "Comparison of multiobjective evolutionary algorithms: Empirical results," *J. Evol. Comput.*, vol. 8, no. 2, pp. 173–195, Jun. 2000.
[41] K. Deb, A. Pratap, S. Agarwal, and T. Meyarivan, "A fast and elitist multiobjective genetic algorithm: NSGA-II," *IEEE Trans. Evol. Comput.*, vol. 6, no. 2, pp. 182–197, Apr. 2002.
[42] Y. Chen, Y. Xu, M. Hu, F. Huang, and Q. Nie, "A 4D-trajectory planning method based on hybrid optimization strategy for demand and capacity balancing," in *Proc. IEEE/AIAA 40th Digit. Avionics Syst. Conf. (DASC)*, Oct. 2021, pp. 1–9.
[43] S. Guo and C. Wu, "Feature weighted association classification algorithm based on statistical harmonic mean," *J. Northwest Univ. Natural Sci. Ed.*, vol. 48, no. 6, pp. 817–826, Jan. 2018.
[44] F. Liu, Z. Li, and H. Xie, "Predicting fuel consumption reduction potentials based on 4D trajectory optimization with heterogeneous constraints," *Sustainability*, vol. 13, no. 13, p. 7013, Jun. 2021.
[45] A. Pellegrini, P. D. Sanzo, B. Bevilacqua, G. Duca, D. Pascarella, R. Palumbo, J. J. Ramos, M. A. Piera, and G. Gigante, "Simulation-based evolutionary optimization of air traffic management," *IEEE Access*, vol. 8, pp. 161551–161570, 2020.
[46] A. Akgunduz, B. Jaumard, and G. Moeini, "Deconflicted air-traffic planning with speed-dependent fuel-consumption formulation," *IEEE Trans. Intell. Transp. Syst.*, vol. 19, no. 6, pp. 1890–1901, Jun. 2018.
[47] W. Zhang, M. Kamgarpour, D. Sun, and C. J. Tomlin, "A hierarchical flight planning framework for air traffic management," *Proc. IEEE*, vol. 100, no. 1, pp. 179–194, Jan. 2012.
[48] J. Meeruang and T. Dolwichai, "Optimum criterion of the vehicle navigation for saving the fuel consumption by Tabu search algorithm with non dominated technique," in *Proc. 8th Int. Conf. Comput. Intell. Commun. Netw. (CICN)*, Dec. 2016, pp. 498–501.

JINLUN ZHOU received the master's degree from the Nanjing University of Aeronautics and Astronautics. His research interest includes trajectory planning.

HONGHAI ZHANG received the Ph.D. degree in engineering. He is currently a Professor with the Nanjing University of Aeronautics and Astronautics, the Director of the Urban Air Traffic Laboratory, Nanjing University of Aeronautics and Astronautics, the Deputy Director of the National Air Traffic Control Flight Flow Management Technology Key Laboratory, and the Deputy Dean of the School of General Aviation and Flight, Nanjing University of Aeronautics and Astronautics.

YUFEI WANG received the master's degree from the Nanjing University of Aeronautics and Astronautics.

Her research interest includes trajectory planning.

GANG ZHONG received the Ph.D. degree in engineering. He is currently a Lecturer with the Nanjing University of Aeronautics and Astronautics.

HAO LIU received the Ph.D. degree in mathematics. He is currently an Associate Professor with the Nanjing University of Aeronautics and Astronautics.